Astrophysical SGWB

Vuk Mandic

Star Formation Rate

Vangioni et al, *MNRAS* 447, 2575 (2015).

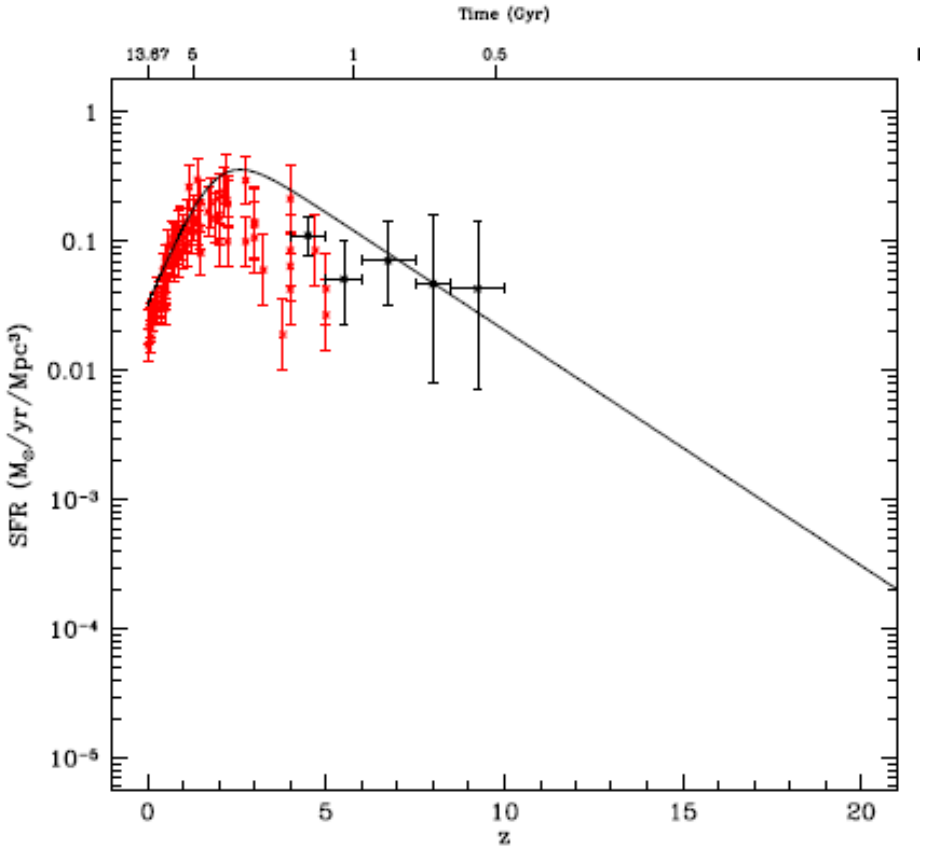

- Many measurements at z < 3, fairly well understood.
- High redshifts are not as well understood, may depend on existence of Pop-3 stars etc.

Time-Delay Distribution

Time-delay distribution (functional form and minimum delay) lead to ~2x variation in the amplitude of the SGWB.

Population synthesis: $P(t) \sim t^{\alpha}$, for $t > t_{min}$:

α = -0.5, -1, -1.5

t_{min} = 20, 100 Myr (BNS)

t_{min} =100, 500 Myr (BBH)

Short GRBs: log-normal distribution.

No time-delay.

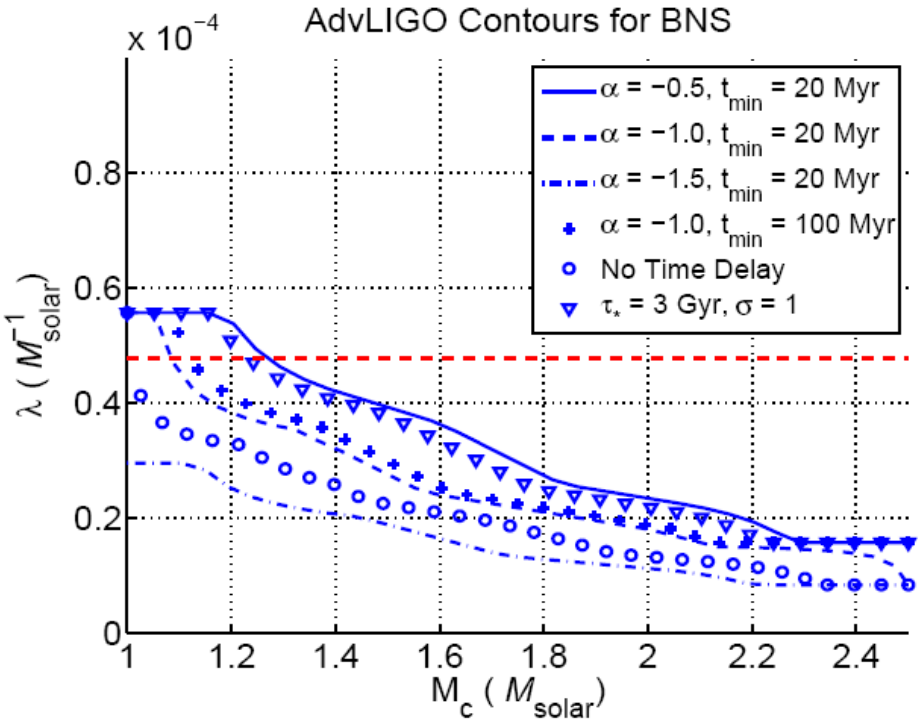

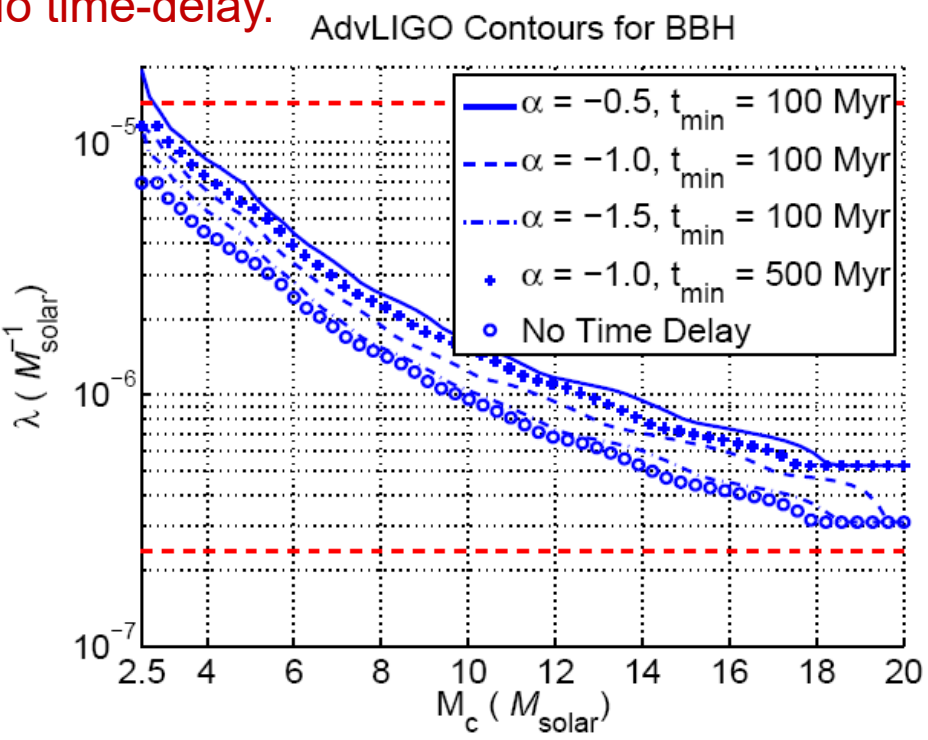

arXiv:2101.12130
LIGO/Virgo O3 isotropic search paper

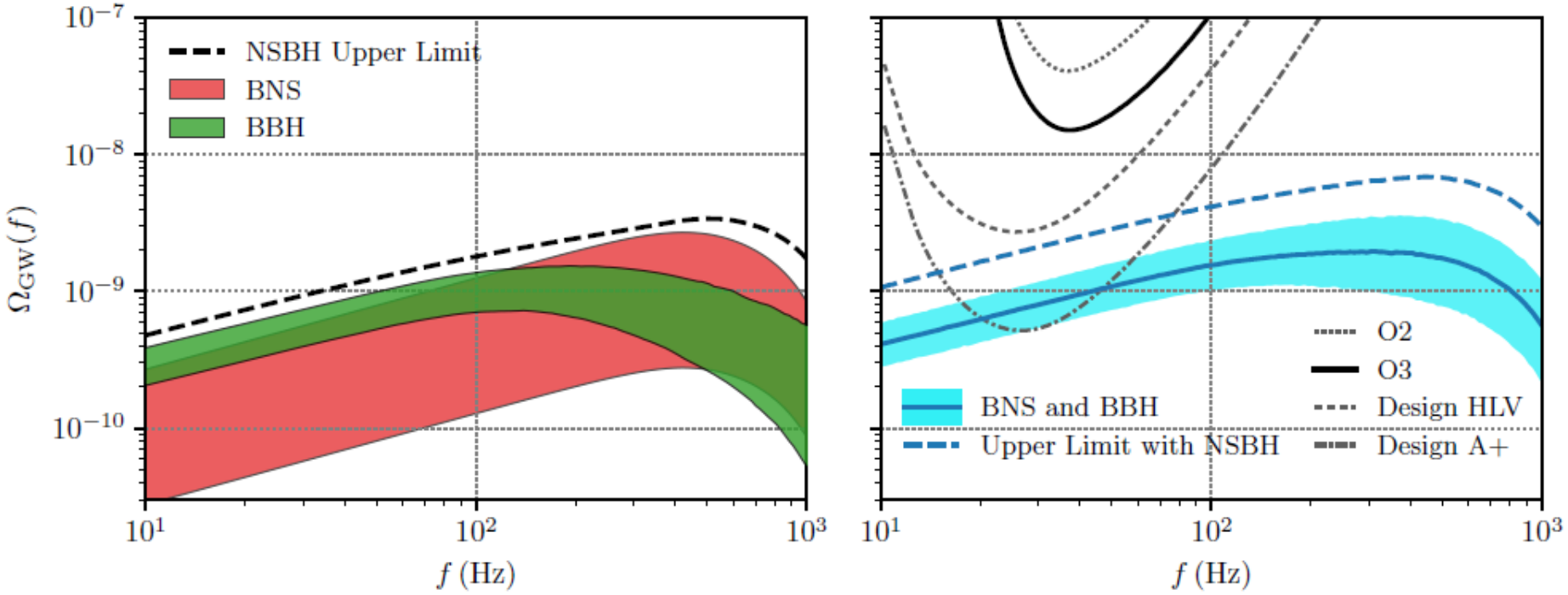

FIG. 5. Fiducial model predictions for the GWB from BBHs, BNSs, and NSBHs, along with current and projected sensitivity curves. In the left panel we show 90% credible bands for the GWB contributions from BNS and BBH mergers. Whereas the BNS uncertainty band illustrates purely the statistical uncertainties in the BNS merger rate, the BBH uncertainty band additionally includes systematic uncertainties in the binary mass distribution, as described in the main text. As no unambiguous NSBH detections have been made, we only show an upper limit on the possible contribution from such systems. The right panel compares the combined BBH and BNS energy density spectra, and 2σ power-law integrated (PI) curves for O2, O3, and projections for the HLV network at design sensitivity, and the A+ detectors. The solid blue line shows the median estimate of $\Omega_{\rm BBH+BNS}(f)$ as a function of frequency, while the shaded blue band illustrates 90% credible uncertainties. The dashed line, meanwhile, marks our projected upper limit on the total GWB, including our upper limit on the contribution from NSBH mergers.

Stellar Core Collapse

Aspherical outflows

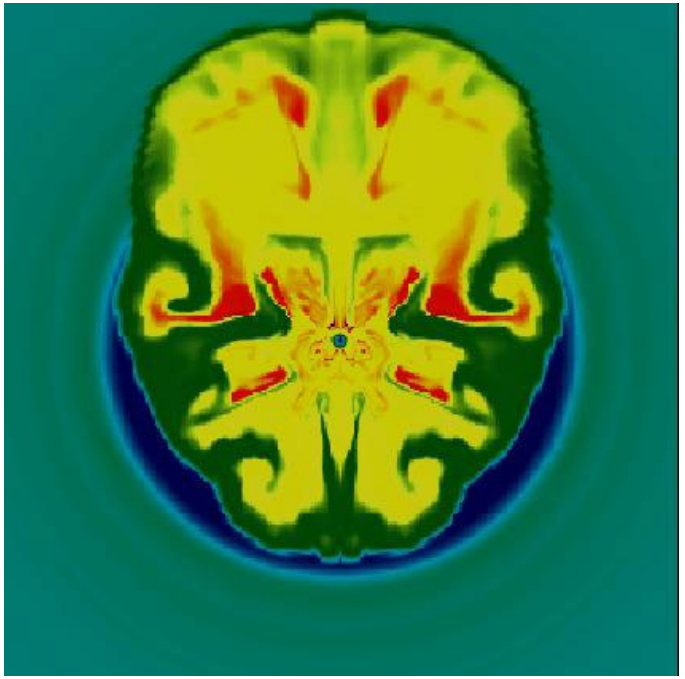

C. Ott

Stellar Core Collapse

Simulations of stellar core collapse GW production yield various predictions

K. Crocker et al, Phys. Rev. D 95, 063015 (2017)

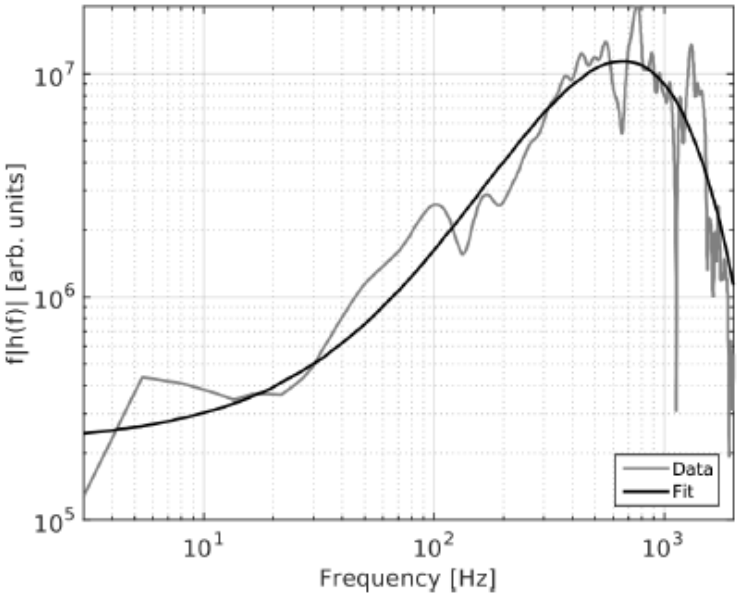

FIG. 4: Plus-polarized gravitational wave signal from an equatorial observation computed in the Abdikamalov et al. `A4006.5` simulation [103]. The original $f|\tilde{h}(f)|$ data is plotted in gray, and the fit to this data (with $a = 82$ Hz and $b = 248$ Hz) of our $f|\tilde{h}(f)|$ model (Eq. 7) is shown in black.

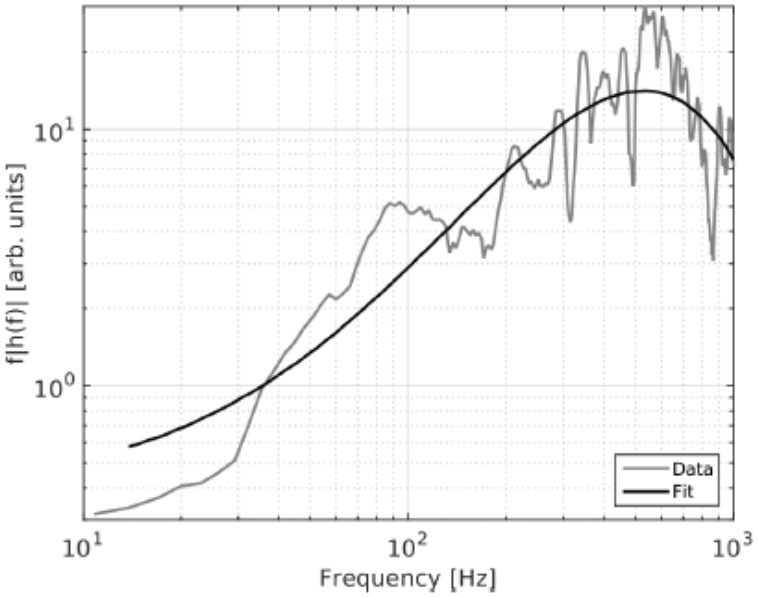

FIG. 6: Gravitational wave signal from an equatorial observation computed by Müller et al. in the `u8.1` simulation [75]. The original $f|\tilde{h}(f)|$ data are plotted in gray, and the fit to these data (with $a = 75$ Hz and $b = 201$ Hz) by our $f|\tilde{h}(f)|$ model (Eq. 7) is shown in black.

Stellar core collapse model: probing the parameter space

K. Crocker et al, Phys. Rev. D 95, 063015 (2017)

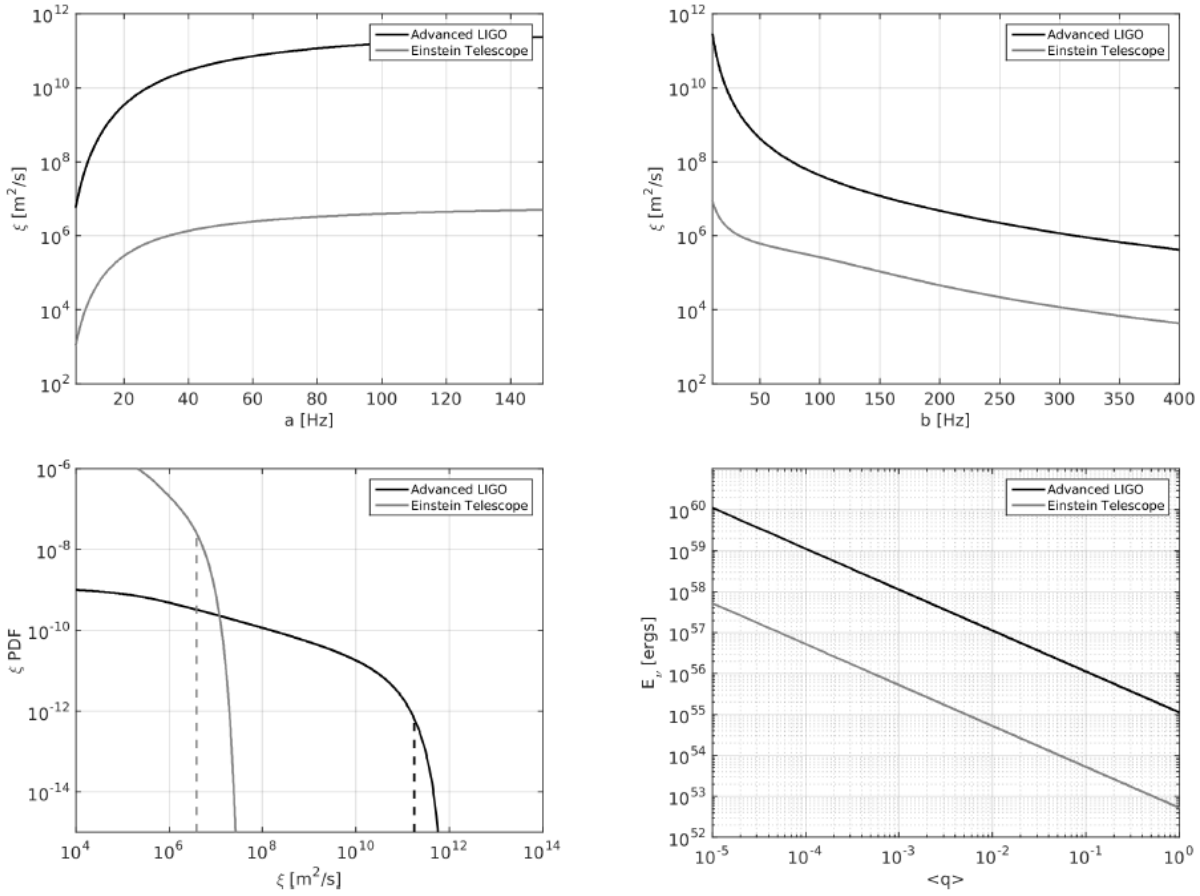

FIG. 9: Top-left: 95% confidence expected sensitivity contours for Advanced LIGO and Einstein Telescope in the ξ-a plane, after marginalizing over the b parameter. Top-right: 95% confidence expected sensitivity contours for Advanced LIGO and Einstein Telescope in the ξ-b plane, after marginalizing over the a parameter. Bottom-left: posterior distribution of ξ after marginalizing over all other parameters; expected sensitivities at 95% confidence are shown as dashed vertical lines. Bottom-right: sensitivity in ξ is translated into sensitivity in the E_ν-$\langle q \rangle$ plane, assuming $\lambda_{\rm CC} \approx 0.01\ {\rm M}_\odot^{-1}$. More details are provided in the text [112].

Magnetar Model

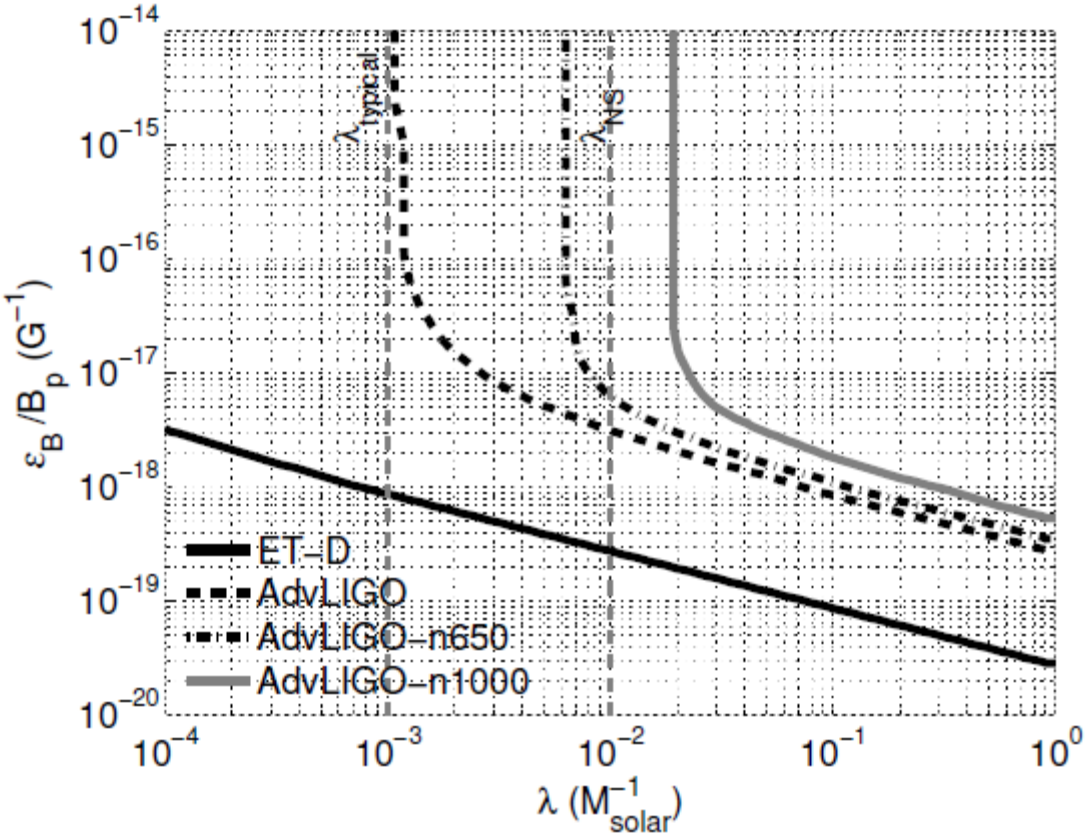

C. Wu et al. Phys. Rev. D 87, 042002 (2013).

Magnetar Model: Poloidal Magnetic Field

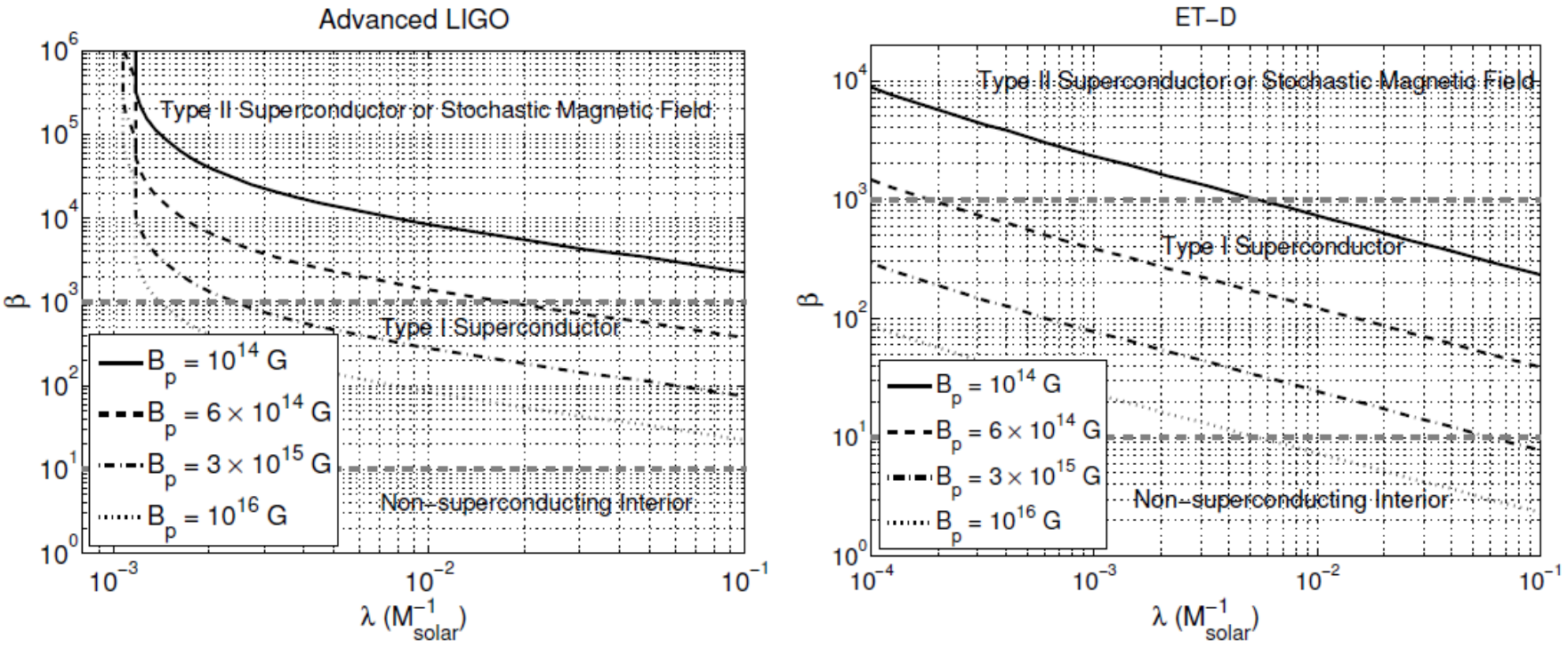

FIG. 5. Sensitivity curves in the $\beta - \lambda$ plane for the poloidal magnetic field configuration with different values of B_p are shown for the second (left) and third (right) generation of GW detectors. We use the star formation rate from Hopkins and Beacom [53] and $P_0 = 1$ ms. The gray horizontal dashed lines denote different types of the equation of state in the interior of magnetars, in the framework of a pure poloidal field configuration.

C. Wu et al. Phys. Rev. D 87, 042002 (2013).

Primordial BBH Model

V. Mandic et al., Phys. Rev. Lett. 117, 201102 (2016).

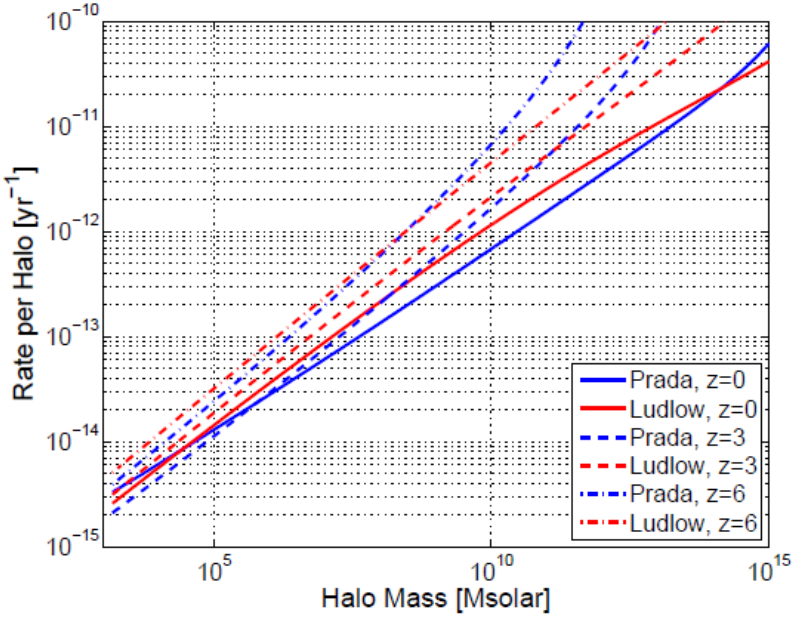

FIG. 1: Primordial BBH merger rate per halo as a function of the halo virial mass for the Prada et al. [34] and Ludlow et al. [33] concentration models, assuming $\lambda = 1$, and for several values of redshift. The local $z = 0$ curves are to be compared to the Figure 1 of [20].

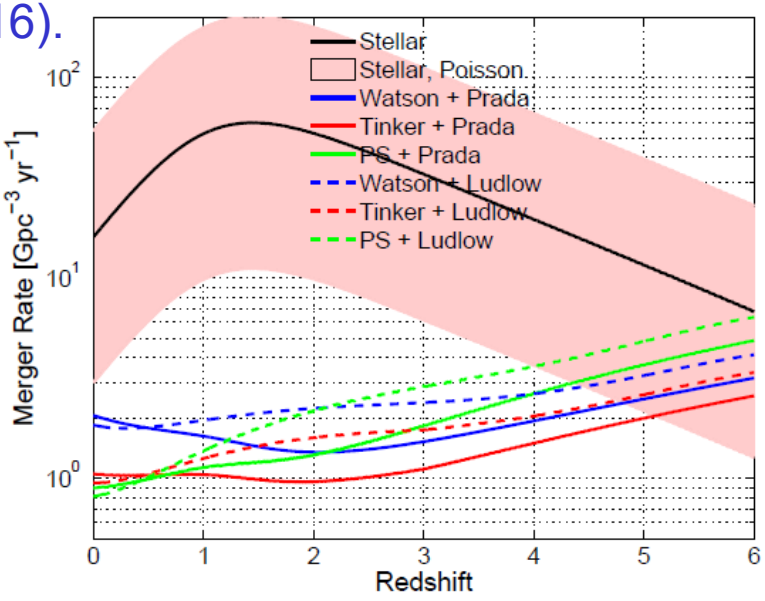

FIG. 2: Primordial BBH merger rate per comoving volume as a function of redshift, using the Prada et al. [34] and Ludlow et al. [33] concentration models, assuming $\lambda = 1$, and for several halo mass function models [36–38]. Note that the fiducial stellar BBH model is computed using black hole binaries which trace the cosmic star formation rate, and thus peaks around $z \sim 1 - 2$ [39]. The Poisson band around the fiducial stellar model represents the statistical uncertainty in the local rate of BBH mergers [39]. The primordial BBH merger rate in all considered models is weakly dependent on redshift and slightly increases with redshift.

Primordial BBH Model

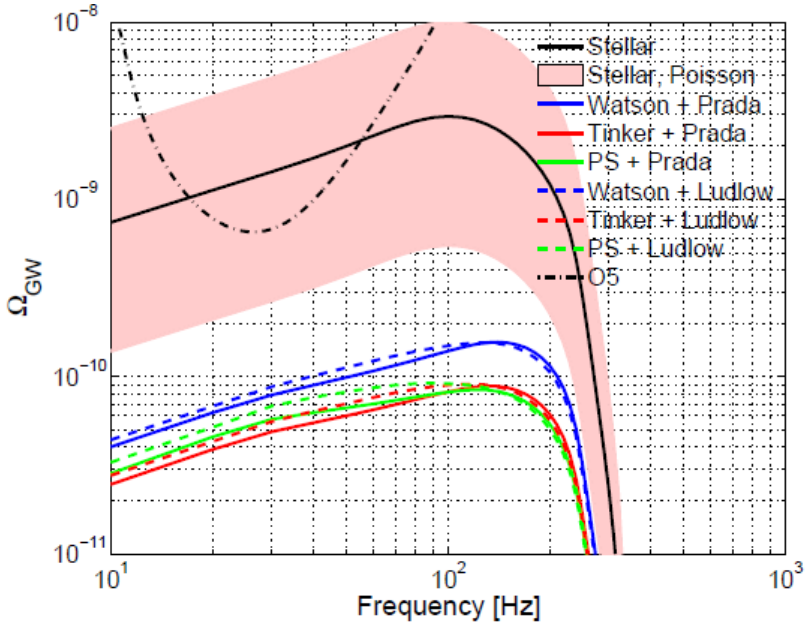

FIG. 3: Gravitational-wave energy density as a function of frequency for the same models of the halo mass function and concentration as considered in Figure 2 and assuming $\lambda = 1$. While different primordial models agree with each other within a factor of ~ 2, the fiducial stellar model is significantly louder. We note that the amplitude of the stellar fiducial model is currently uncertain due to the large errors on the local rate of BBH mergers, as denoted by the Poisson band [39]. Also shown is the projected final sensitivity of advanced detectors, denoted O5 [39].

V. Mandic et al., Phys. Rev. Lett. 117, 201102 (2016).

- Assumes all BBH masses are the same as for GW150914.
- Do not expect significant difference when using more realistic BBH mass distributions.

Stochastic Background of Gravitational Waves

- Energy density:

$$\rho_{GW} = \frac{c^2}{32\pi G} < \dot{h}_{ab}\, \dot{h}^{ab} >$$

- Characterized by log-frequency spectrum:

$$\Omega_{GW}(f) = \frac{1}{\rho_c} \frac{d\rho_{GW}(f)}{d \ln f}$$

- Related to the strain power spectrum:

$$S(f) = \frac{3H_0^2}{10\pi^2} \frac{\Omega_{GW}(f)}{f^3}$$

- Strain scale:

$$h(f) = 6.3 \times 10^{-22} \sqrt{\Omega_{GW}(f)} \left(\frac{100 \text{ Hz}}{f}\right)^{3/2} \text{Hz}^{-1/2}$$

Detection Strategy

- Cross-correlation estimator

$$Y = \int_{-T/2}^{+T/2} dt_1 \int_{-T/2}^{+T/2} dt_2 \; s_1(t_1) \; s_2(t_2) \; Q(t_2 - t_1)$$

$$Y = \int_{-\infty}^{+\infty} df \; \tilde{s}_1^*(f) \; \tilde{s}_2(f) \; \tilde{Q}(f)$$

- Theoretical variance

$$\sigma_Y^2 \approx \frac{T}{2} \int_0^{+\infty} df \; P_1(f) \; P_2(f) \; | \; \tilde{Q}(f) \; |^2$$

- Optimal Filter

$$\tilde{Q}(f) = \frac{1}{N} \; \frac{\gamma(f) \; \Omega_t(f)}{f^3 \; P_1(f) \; P_2(f)}$$

Overlap Reduction Function

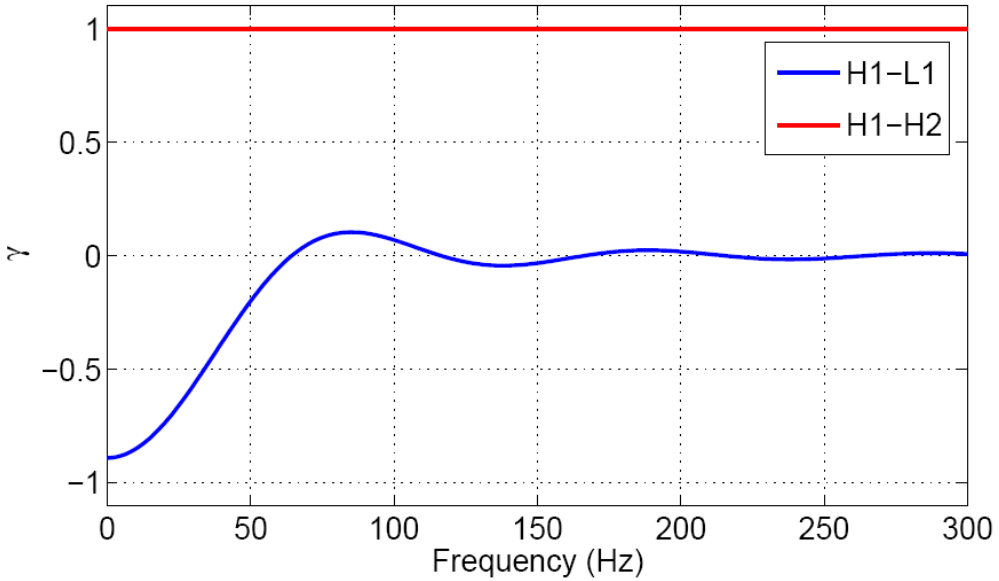

For template: $\Omega_t(f) = \Omega_\alpha (f/100 \text{ Hz})^\alpha$

Choose *N* such that: $\langle Y \rangle = \Omega_\alpha T$

O3 Result: Pre-processing

- Time-series data are sampled at 16384 Hz.
  - » Downsample to 4096 Hz, so Nyquist frequency is 2048 Hz.
  - » Analyze data below 1726 Hz to avoid aliasing effects.
- High-pass filter is applied to remove the low-frequency noise (16th-order Butterworth filter, with a knee frequency of 11 Hz)
- Divide data into time segments of duration T=192 s.
  - » Hann-windowed and overlapped by 50%.
- Compute discrete Fourier transform on each segment.
- Coarse-grain the spectrum 1/32 Hz.

O3 Data Quality

- Stationarity cut
  - » Remove noise fluctuations that cause >20% variations in σ_Y from segment to segment.
  - » These segments can have inaccurate estimates of the PSD or of Y(f), so we remove them. Typically lose 4-5% of the data.
- Frequency notching
  - » 60 Hz harmonics, violin modes, calibration lines, 1 Hz harmonics
  - » Occasionally observe beating of two lines
  - » Eliminate ~10% of the frequency band.

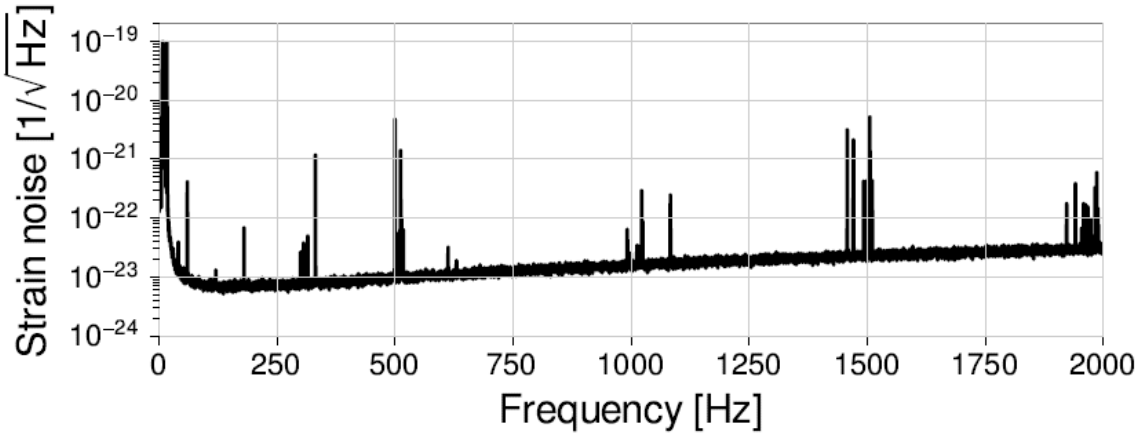

LLO, 2017
arXiv:1908.11170

O3 Data Quality: Gating

- In O3, observed many loud glitches.
- Stationarity cut was expensive, losing >50% of the data.
- Gating procedure: Identify glitch time, then nullify the time series.

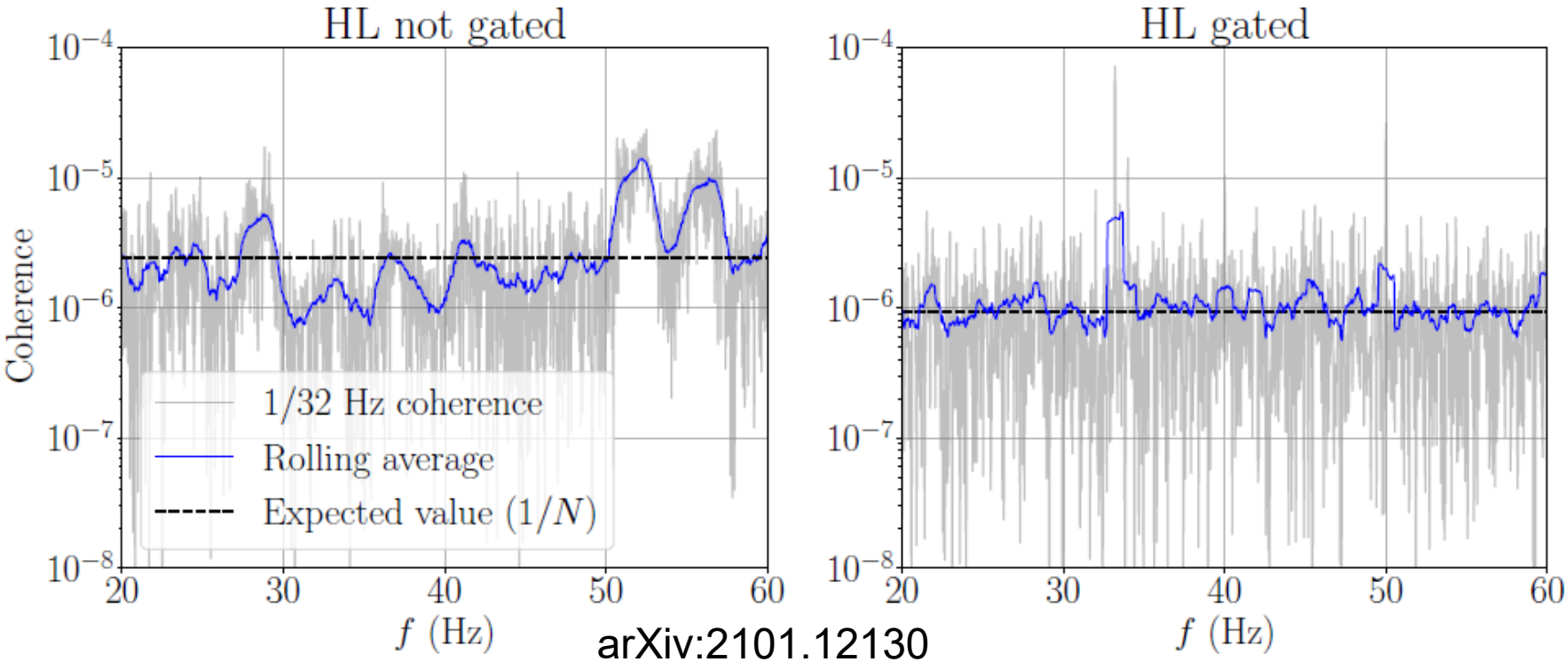

arXiv:2101.12130

O3 Data Quality: Magnetic Noise

- Magnetic noise can be globally correlated on Earth.
  - » Schumann resonances: standing waves in the resonant cavity between the Earth and the ionosphere, generated by storms.
- If magnetic field couples to GW detectors, this could generate correlated noise between GW detectors.
- Approach 1:
  - » Measure magnetic coupling via injections.
  - » Measure magnetic correlations between sites.
  - » Combine into a prediction of the magnetic contribution to Ω_{GW}.
- Approach 2:
  - » Model the magnetic contamination.
  - » Estimate it simultaneously with the SGWB in a Bayesian parameter estimation framework.

O3 Data Quality: Magnetic Noise

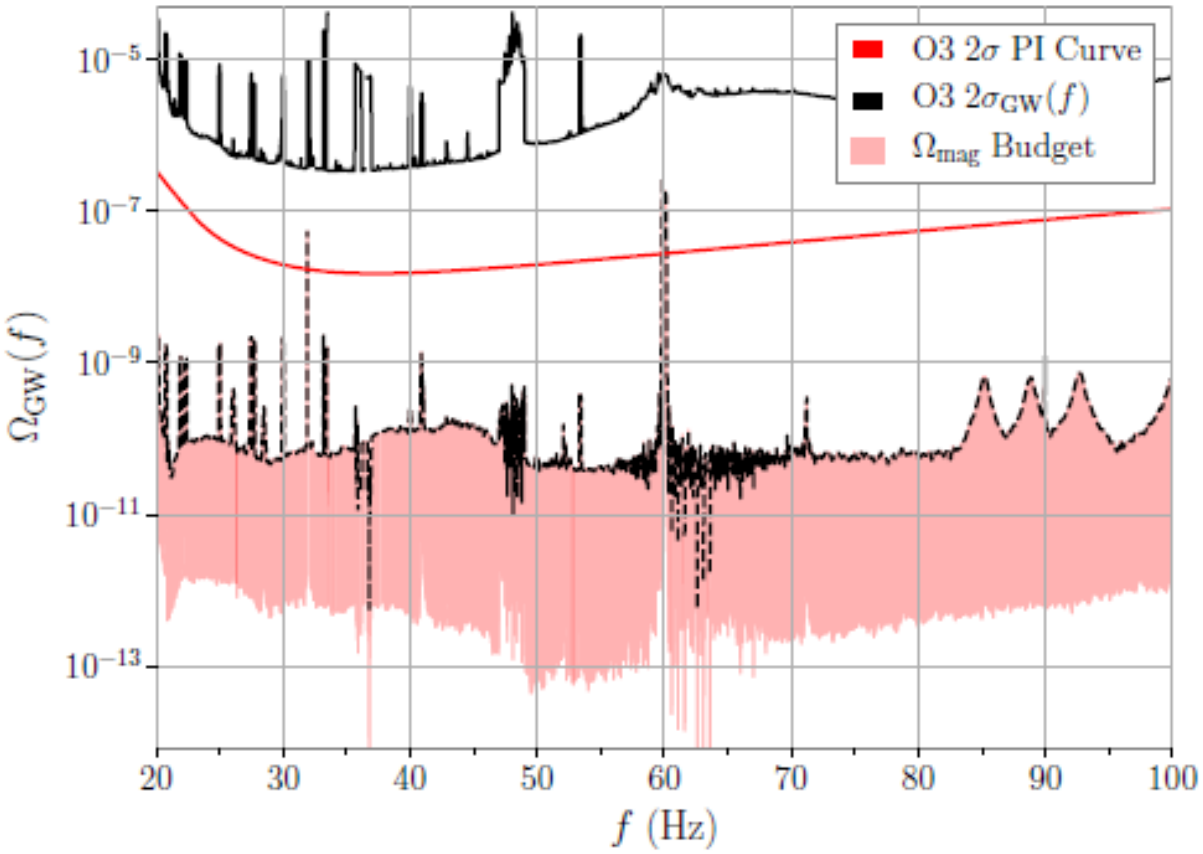

arXiv:2101.12130

O3(+O2+O1) Results

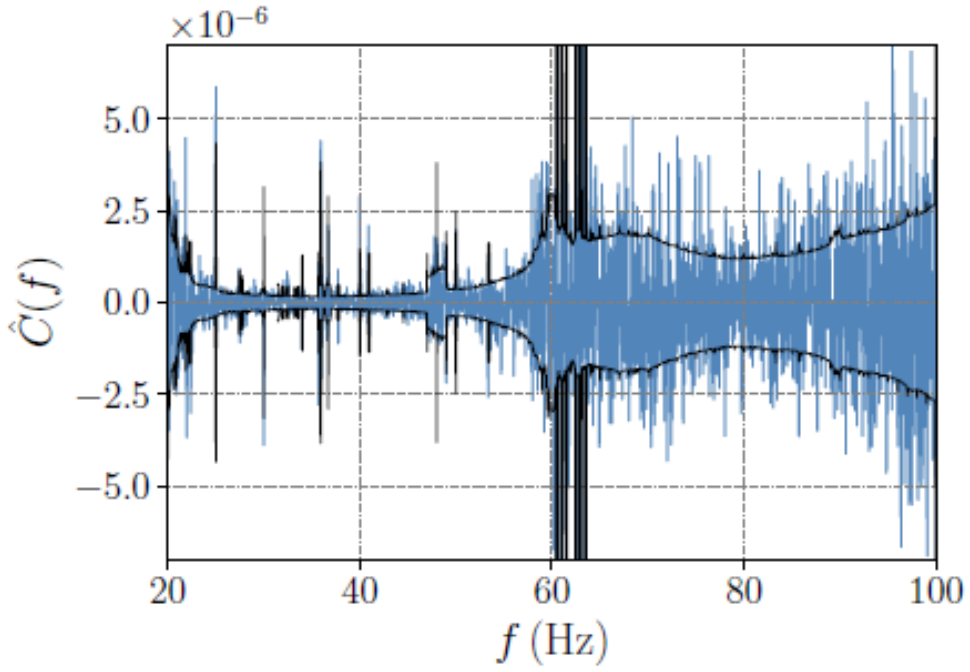

- Observed cross-correlation spectrum is consistent with noise.
- Place upper limits on Ω_α for different power law indices α.
- Adding magnetic noise to the model reduces the Bayes factor (prefers the no-magnetic-noise model).

arXiv:2101.12130

	Uniform prior			Log-uniform prior		
α	O3	O2 [43]	Improvement	O3	O2 [43]	Improvement
0	1.7×10^{-8}	6.0×10^{-8}	3.6	5.8×10^{-9}	3.5×10^{-8}	6.0
2/3	1.2×10^{-8}	4.8×10^{-8}	4.0	3.4×10^{-9}	3.0×10^{-8}	8.8
3	1.3×10^{-9}	7.9×10^{-9}	5.9	3.9×10^{-10}	5.1×10^{-9}	13.1
Marg.	2.7×10^{-8}	1.1×10^{-7}	4.1	6.6×10^{-9}	3.4×10^{-8}	5.1

O3(+O2+O1) Results

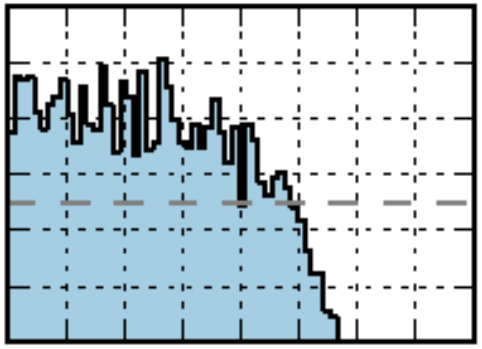

Can perform 2D fit to estimate both amplitude and power index.

$$\Omega_{\mathrm{GW}}(f) = \Omega_{\mathrm{ref}} \left(\frac{f}{f_{\mathrm{ref}}} \right)^{\alpha}$$

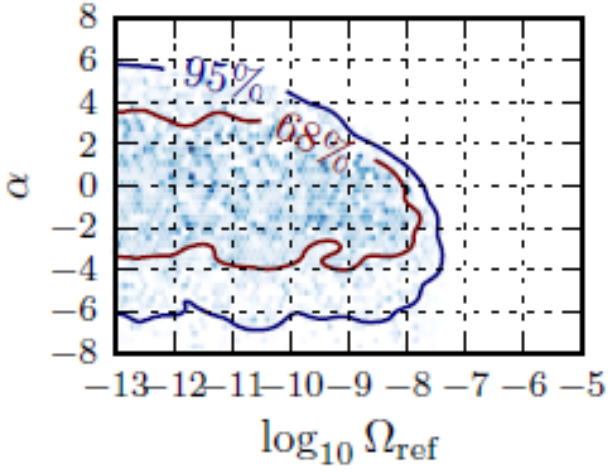

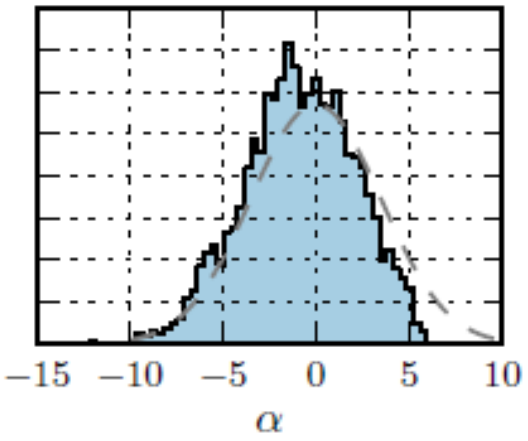

Polarized Background

- Examples of overlap reduction functions for polarized SGWB background.

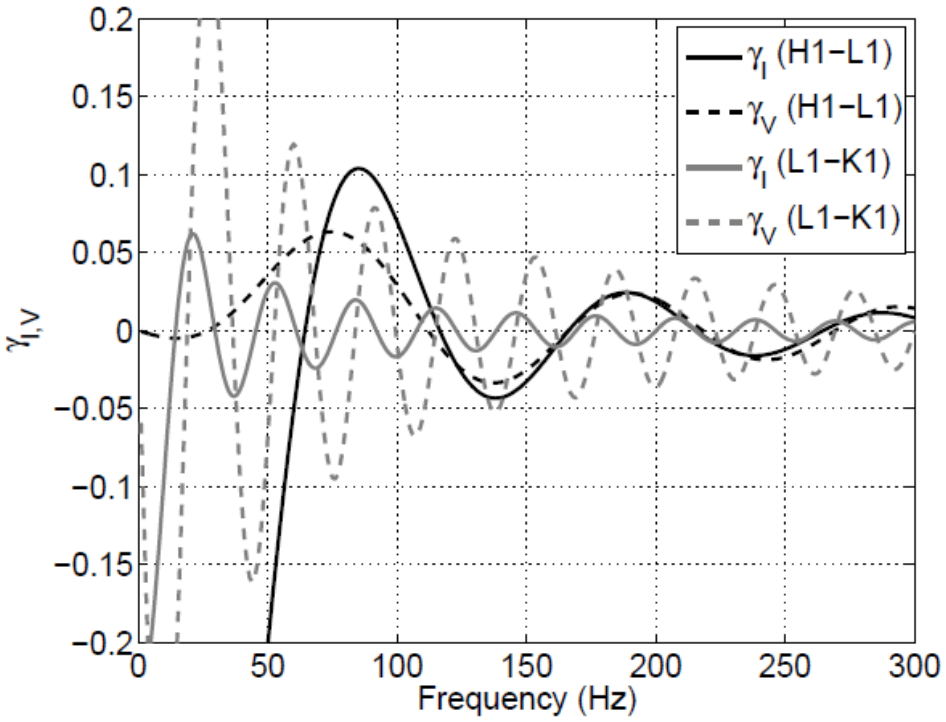

Crowder et al., Phys. Lett. B 726, 66 (2013)

Polarized Background

Crowder et al., Phys. Lett. B 726, 66 (2013)

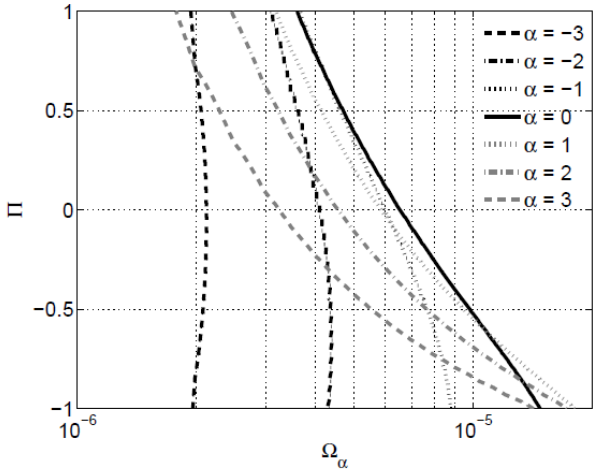

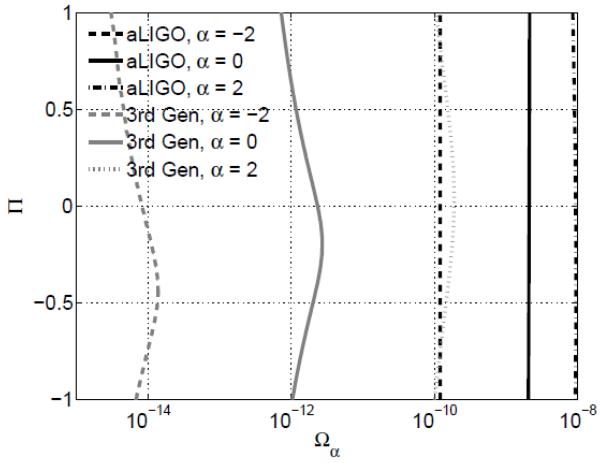

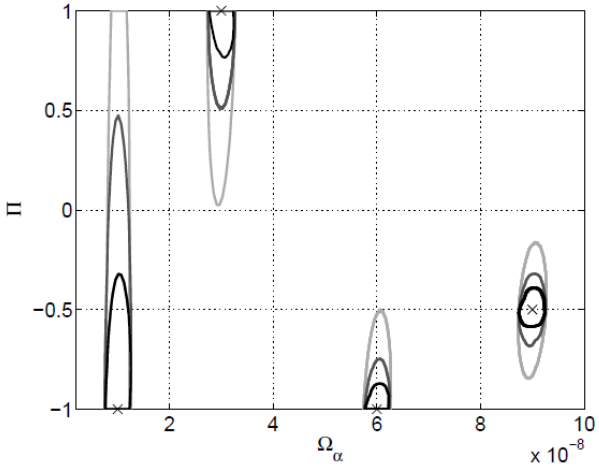

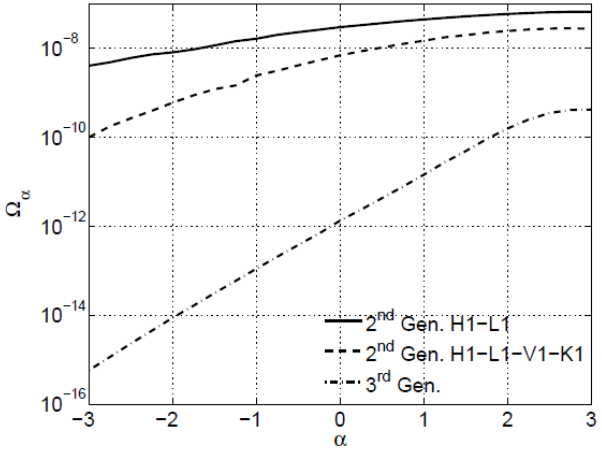

Anisotropic Searches

- Measure from where (on the sky) the signal comes from.
  - » Time-delay between two detectors.
  - » Earth rotation breaks degeneracies for permanent signals.
- Redefine energy density:

$$\Omega_{\rm GW}(f) \equiv \frac{f}{\rho_c}\frac{d\rho_{\rm GW}}{df} = \frac{2\pi^2}{3H_0^2} f^3 \int_{S^2} d\hat{\Omega}\, \mathcal{P}(f,\hat{\Omega})$$

- Point source (radiometer) search: $\mathcal{P}(\hat{\Omega}) \equiv \eta(\hat{\Omega}_0)\, \delta^2(\hat{\Omega}, \hat{\Omega}_0)$

- Spherical harmonic decomposition (similar to CMB analyses):

$$\mathcal{P}(\hat{\Omega}) \equiv \sum_{lm} \mathcal{P}_{lm} Y_{lm}(\hat{\Omega})$$

SGWB Directionality: Radiometer and Sph. Harmonics

- Cosmological SGWB likely isotropic.
- Astrophysical SGWB might be anisotropic.
  - » Point sources.
  - » Extended sources (e.g. Milky Way).
- Have pipelines to deal with both:
  - » Radiometer.
  - » Spherical harmonics decomposition.

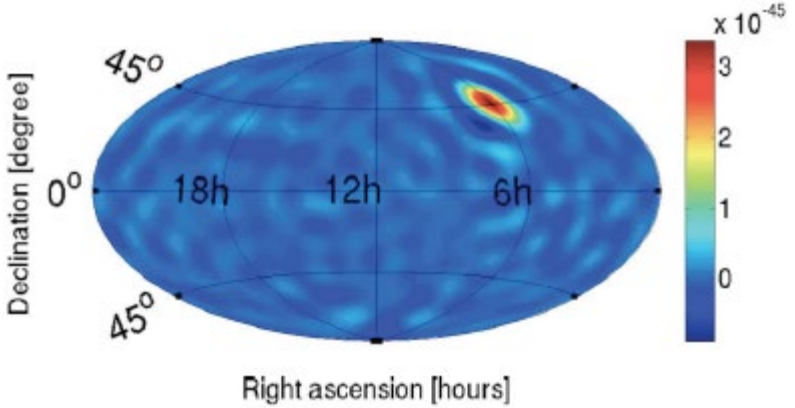

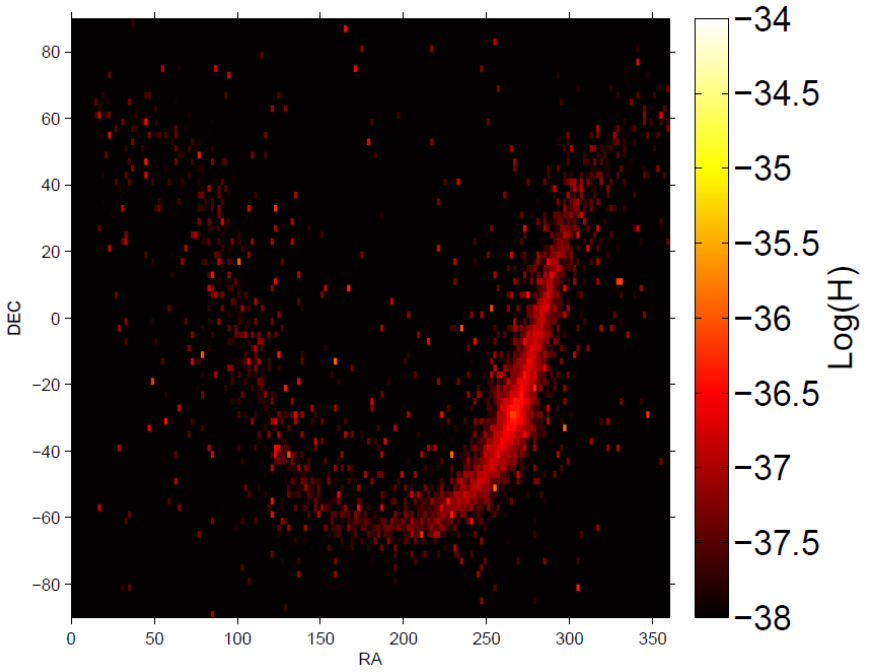

Anirban Ain: simulation of a point source

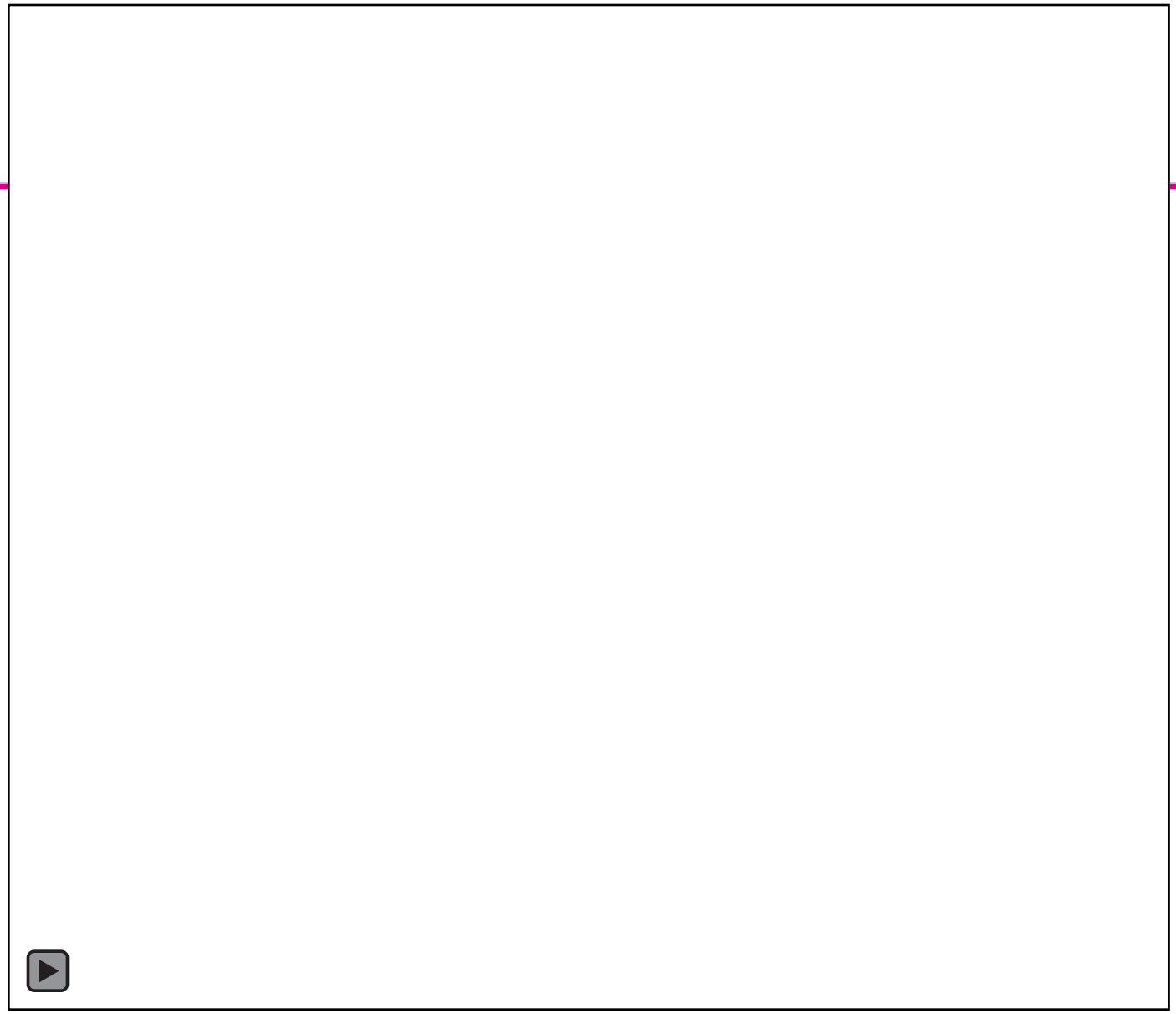

Anirban Ain: simulation of an extended source

Regularization

- Diagonalize the Fisher matrix to find eigenvalues.
  - » Note the eigenvalues significantly drop.
- Replace these with infinity, allows the matrix to be inverted.
- Adding third detector helps regularize the overall Fisher matrix.

arXiv:2103.08520

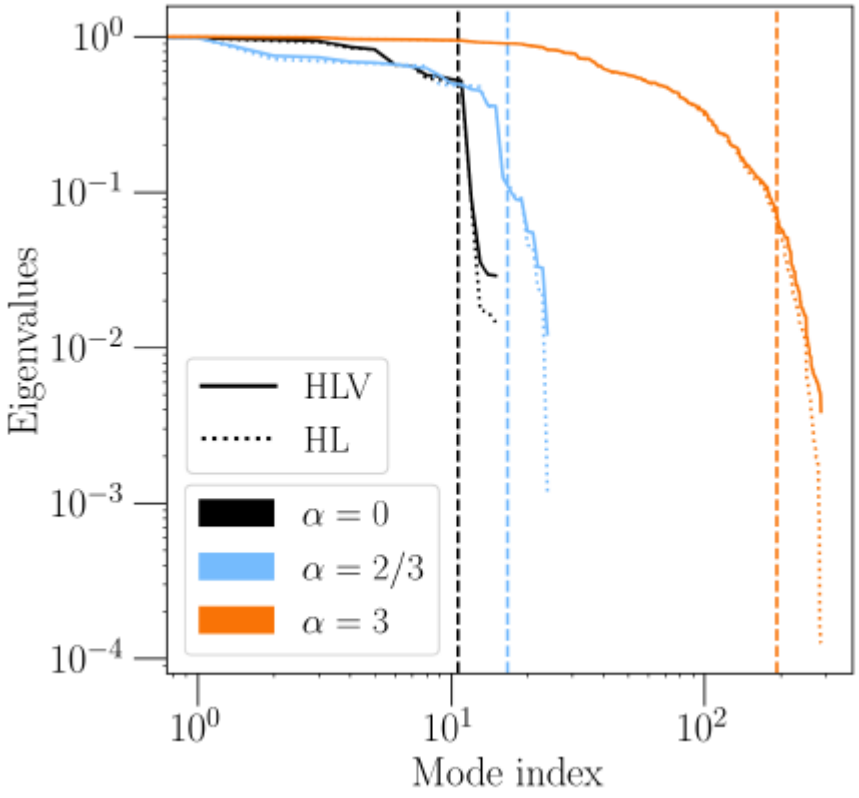

Anisotropic Signal Simulations

Anisotropic stochastic signal added to the data (in software or hardware) and successfully recovered.

WMAP map added to data in software
E. Thrane et al, Phys. Rev. D 80, 122002 (2009).

Point source simulation in hardware
M. Pihlaja's M.S. Thesis (2011).

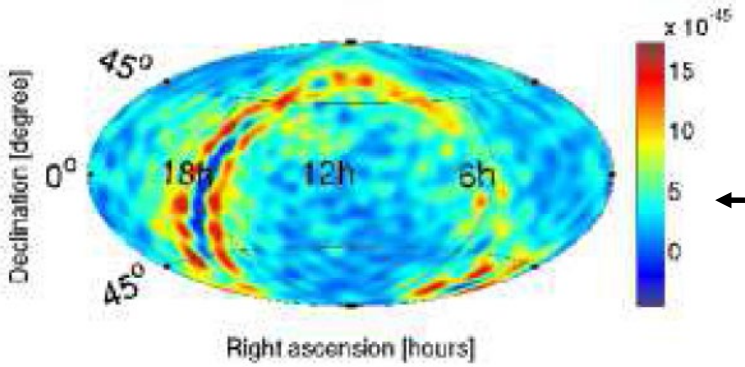

Injected

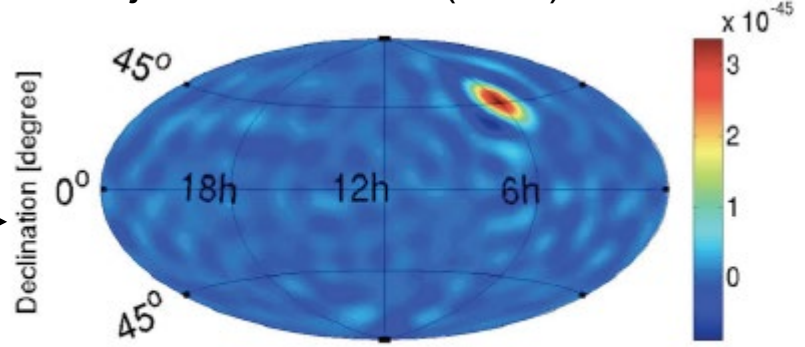

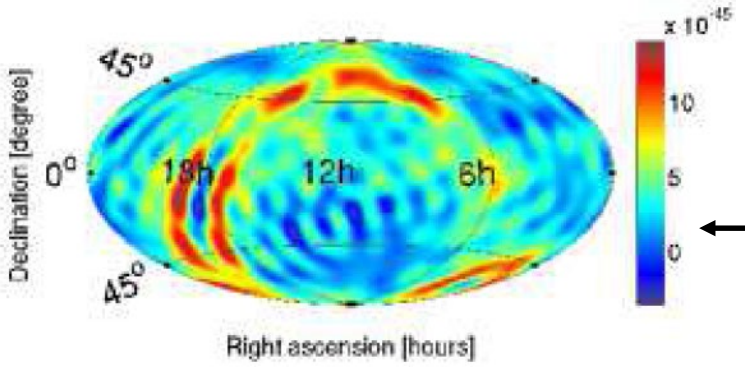

Recovered

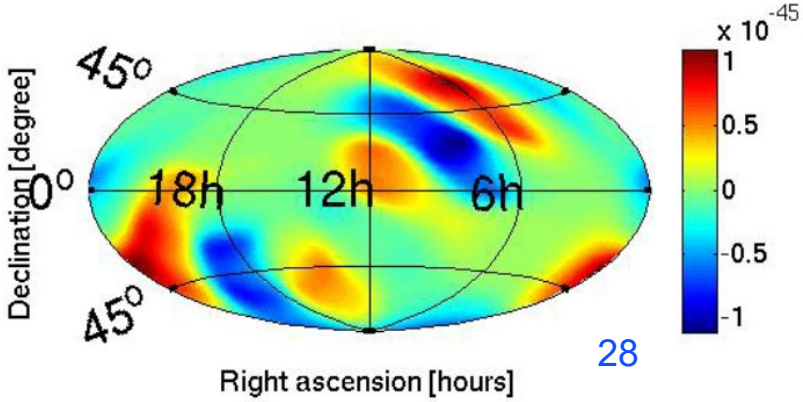

O1-O3 Broadband Radiometer Search

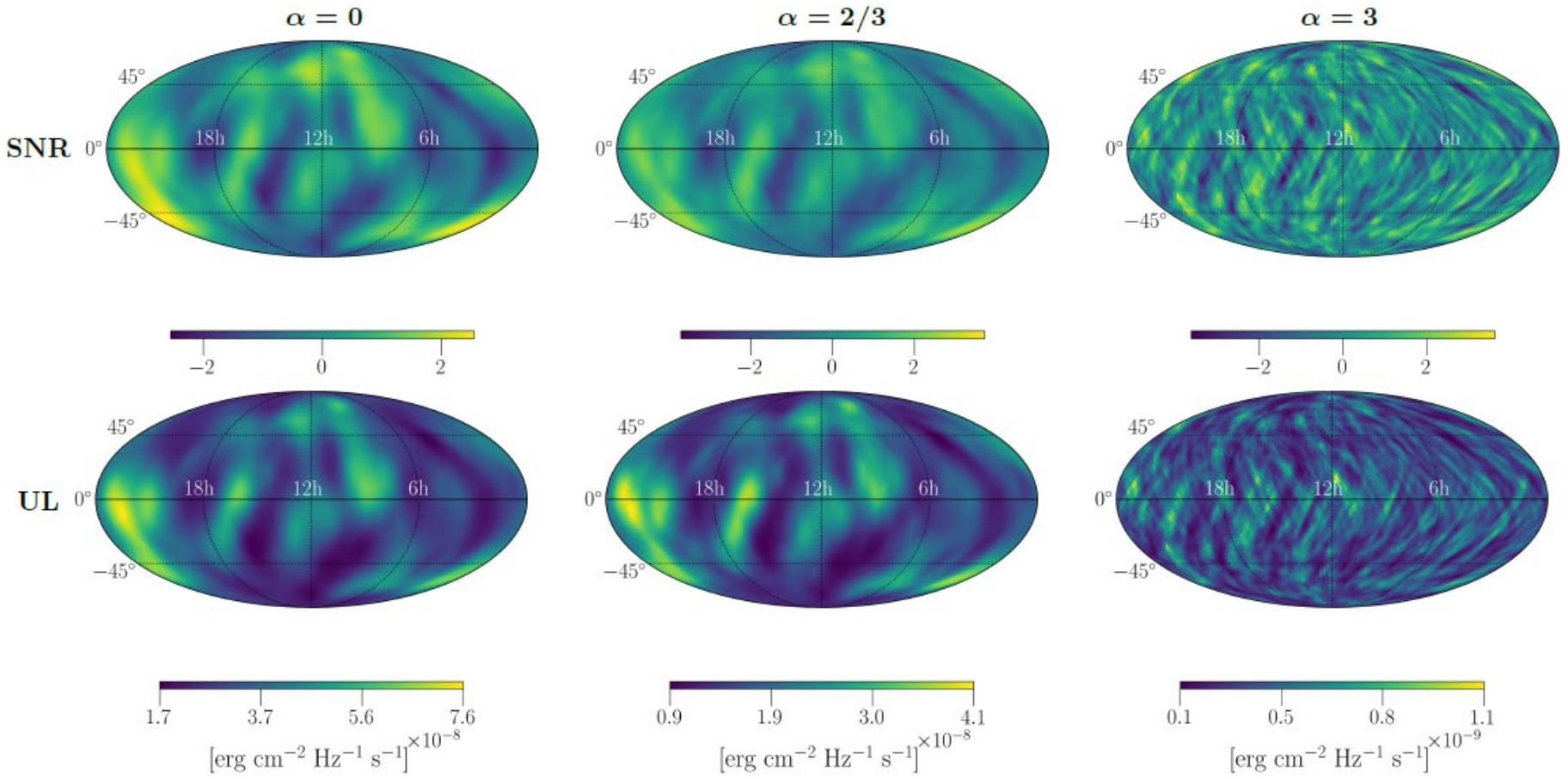

arXiv:2103.08520

O1-O3 Broadband Radiometer Search

- Performed in pixel basis, but integrating over a broad (20-1726 Hz) frequency band.
- Repeated for different spectral (power-law) indices.

All-sky BBR Results

			Max SNR (% p-value)				Upper limit ranges (10^{-8})	
α	Ω_{GW}	$H(f)$	HL(O3)	HV(O3)	LV(O3)	O1+O2+O3 (HLV)	O1+O2+O3 (HLV)	O1 + O2 (HL)
0	constant	$\propto f^{-3}$	2.3 (66)	3.4 (24)	3.1 (51)	2.6 (23)	1.7 – 7.6	4.5 – 21
2/3	$\propto f^{2/3}$	$\propto f^{-7/3}$	2.5 (59)	3.7 (14)	3.1 (62)	2.7 (24)	0.85 – 4.1	2.3 – 12
3	$\propto f^{3}$	constant	3.7 (32)	3.6 (47)	4.1 (12)	3.6 (20)	0.013 – 0.11	0.047 – 0.32

arXiv:2103.08520

O1-O3 Spherical Harmonics Decomposition

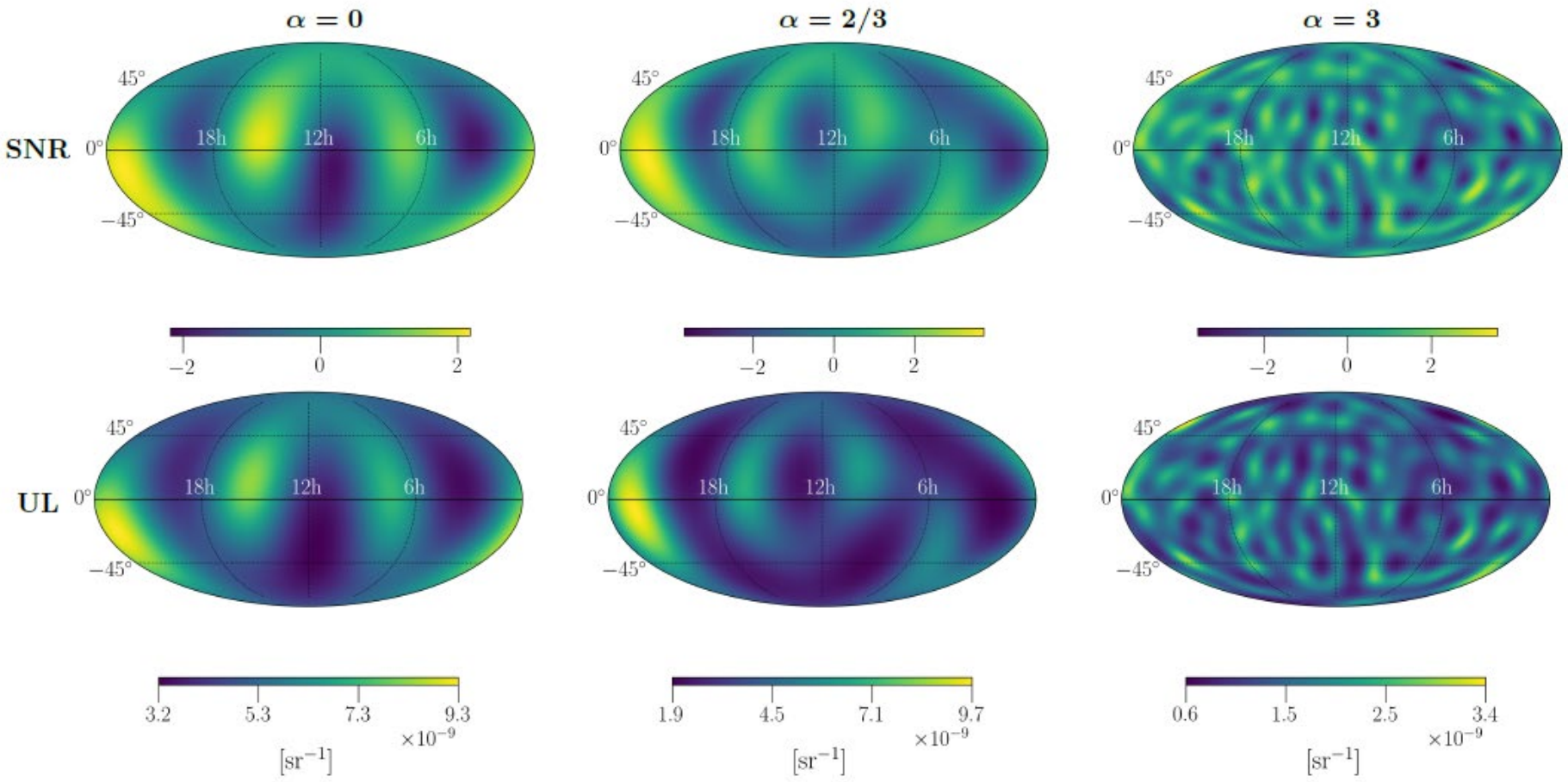

arXiv:2103.08520

O1-O3 Spherical Harmonics Decomposition

SHD Results

			Max SNR (% p-value)				Upper limit range (10^{-9})	
α	Ω_{GW}	$H(f)$	HL(O3)	HV(O3)	LV(O3)	O1+O2+O3 (HLV)	O1+O2+O3 (HLV)	O1 + O2 (HL)
0	constant	$\propto f^{-3}$	1.6 (78)	2.1 (40)	1.5 (83)	2.2 (43)	3.2–9.3	7.8–29
2/3	$\propto f^{2/3}$	$\propto f^{-7/3}$	3.0 (13)	3.9 (0.98)	1.9 (82)	3.7 (1.7)	1.9–9.7	6.5–25
3	$\propto f^{3}$	constant	3.9 (12)	4.0 (10)	3.9 (11)	3.2 (60)	0.56–3.4	1.9–11

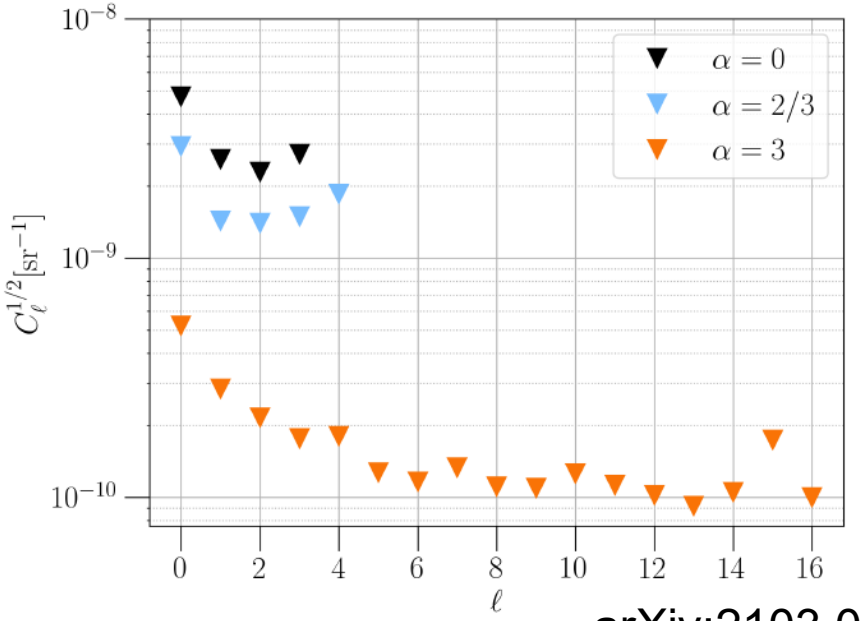

- Repeated for different power-law index α.
- Note that different α values emphasize different frequencies.
  - » Implies different angular resolution and maximum l for the spherical harmonic decomposition.

arXiv:2103.08520

O1-O3 Narrowband Radiometer Search

- For specific promising point-source directions, complete frequency-dependent analysis.
  - » Can search for narrowband (line) searches in these directions.
  - » Computationally expensive, not done for all directions on the sky.
  - » New search: All-sky-all-frequencies (ASAF) currently pursued.

Narrowband Radiometer Results

Direction	Max SNR	p-value (%)	Frequency (Hz) ($\pm$ 0.016 Hz)	Best upper limit (10^{-25})	Frequency band (Hz)
Sco X-1	4.1	65.7	630.31	2.1	189.31 – 190.31
SN 1987A	4.9	1.8	414.0	1.7	185.13 – 186.13
Galactic Center	4.1	62.3	927.25	2.1	202.56 – 203.56

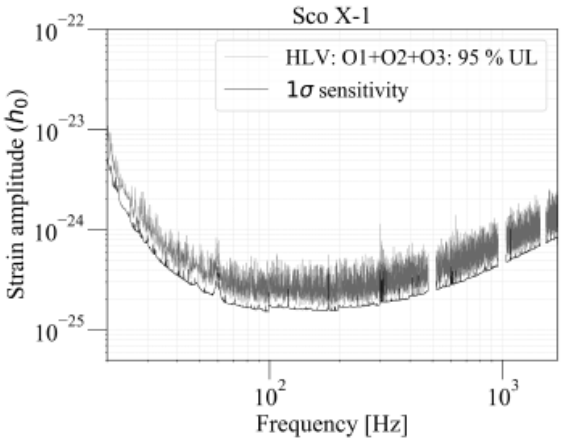

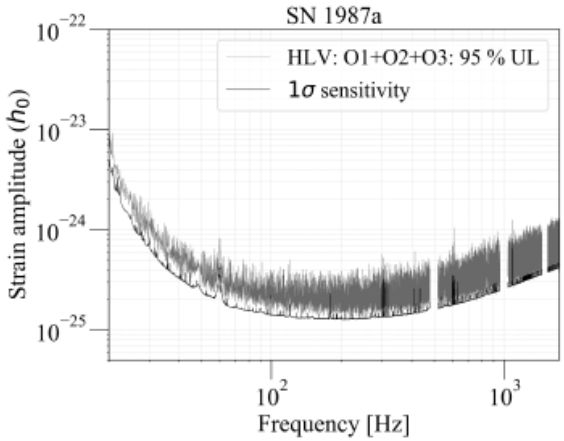

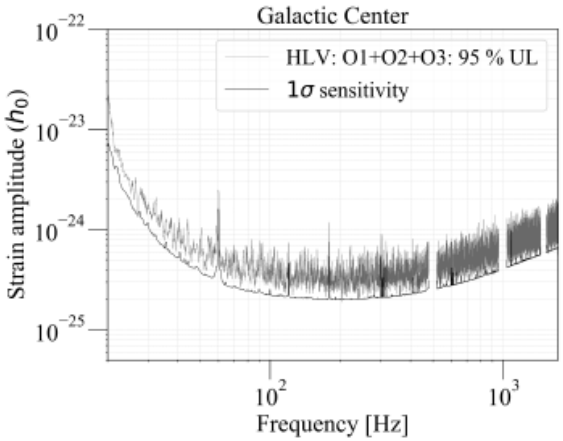

Angular Resolution

- Past searches use “diffraction limit” to define the angular resolution:

$$\theta = \frac{c}{2Df} \qquad \ell_{\max} = \frac{\pi}{\theta}$$

- We integrate over frequency, so searches pick the “most sensitive frequency” for a given α.
  - » f = 50 Hz implies l_{max} = 3-4.
- Diffraction limit refers to the size of a receiver relative to the observed wavelength.
- But in our directional searches, we use the **time delay between 2 receivers** to extract directional information.
  - » Is it appropriate to use the diffraction limit?
  - » We include f > 50 Hz – shouldn’t this imply some angular sensitivity at *l* > 3?

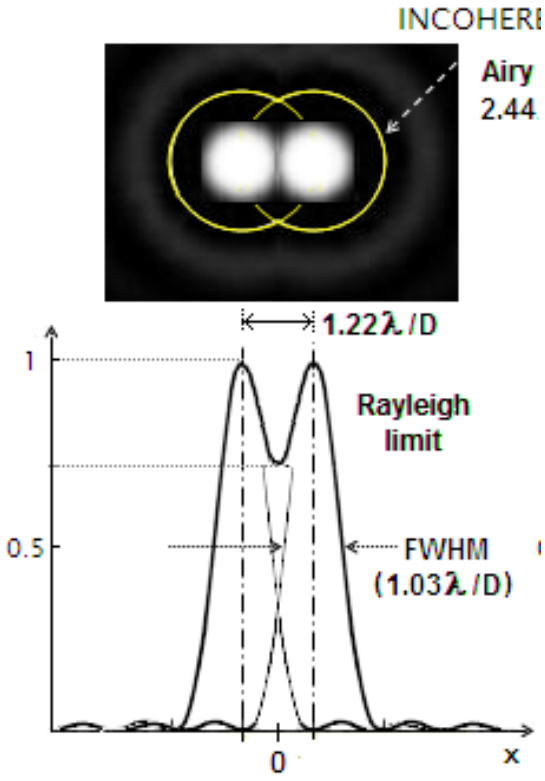

Intuition: Toy Model

- Imagine two buoys measuring the water wave height, assume a single plane wave.
  - » Vary the SNR of the buoy measurements.
  - » Infinite SNR means measuring perfectly the wave profile at each buoy, hence measuring perfectly the time-delay between two buoys, hence measuring perfectly the wave direction.

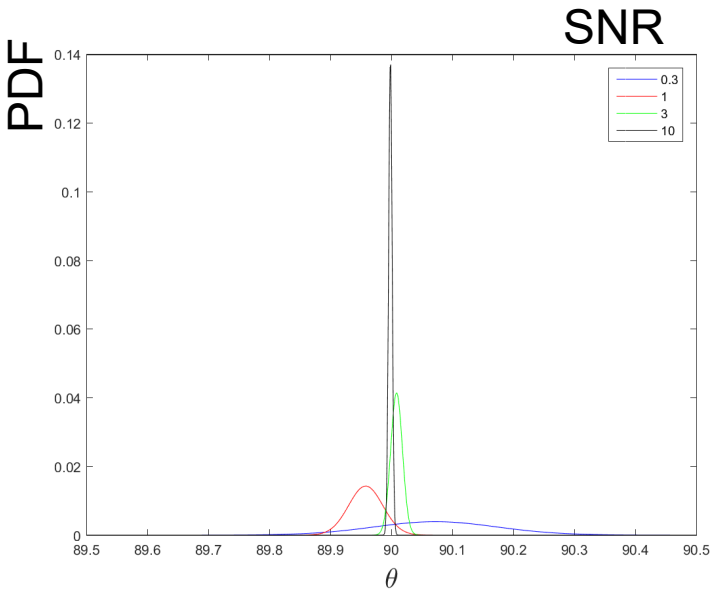

Intuition: Toy Model

- If nature sends a **single plane wave**, and we search for a **single plane wave** with **infinite SNR** buoys, we can extract the wave direction with zero error.
  - » Beating the diffraction limit!
- What if nature sends two plane waves at the same frequency?
  - » Two sine waves add to make another sine wave with a different phase!
    - – May be able to distinguish them with a smarter algorithm, explicitly searching for two waves…
    - – If sources emit multiple frequencies, could use this too…
  - » What if there are more than 2 waves? What algorithm should we use?
- What if the waves do not originate from point sources, but are instead coming from extended objects on the sky?

Buoy Radiometer

Andrew Matas

- Andrew Matas: derived the full radiometer formalism for two buoys rotating around midpoint.
  - » Both for isotropic and “lighthouse” response.
- In isotropic response case, Fisher matrix proportional to the Bessel function:

$$\Gamma_{mn} = \frac{1}{4P_0^2} J_n(2\pi f L/c)^2 N_S \delta_{mn}$$

- Peaks at n ~ 2π f D/c, the usual diffraction limit.
- In “lighthouse” response case, can beat the diffraction limit:

$$\Gamma_{nm} = \frac{1}{4}\delta_{nm}\delta(\varphi_1, \varphi_2)^2$$

- Also recovered the single point source result:
  - » Angular resolution scales as SNR^{-1}.

Theoretical Modeling of Anisotropy: Compact Binaries

- Predictions by multiple author groups:
  - » G. Cusin et al.
  - » M. Sakellariadou et al.
- Astrophysical Kernel as a function of redshift and GW frequency:

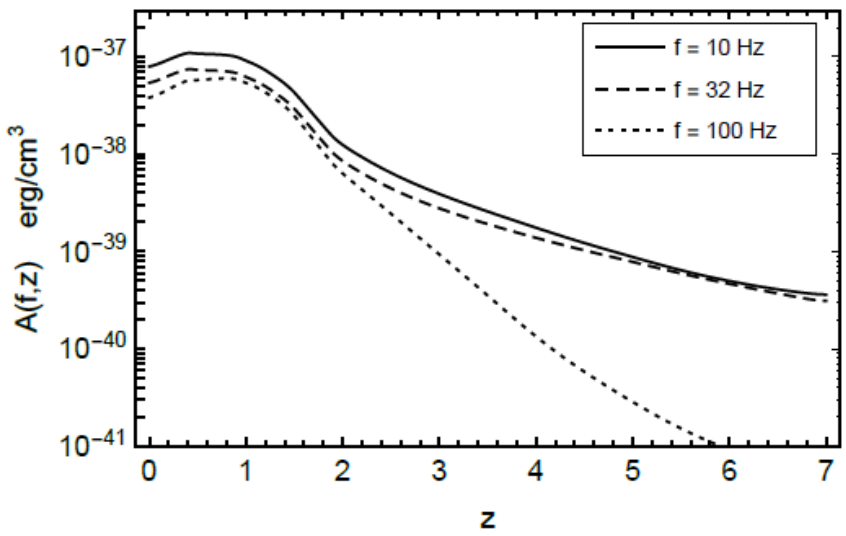

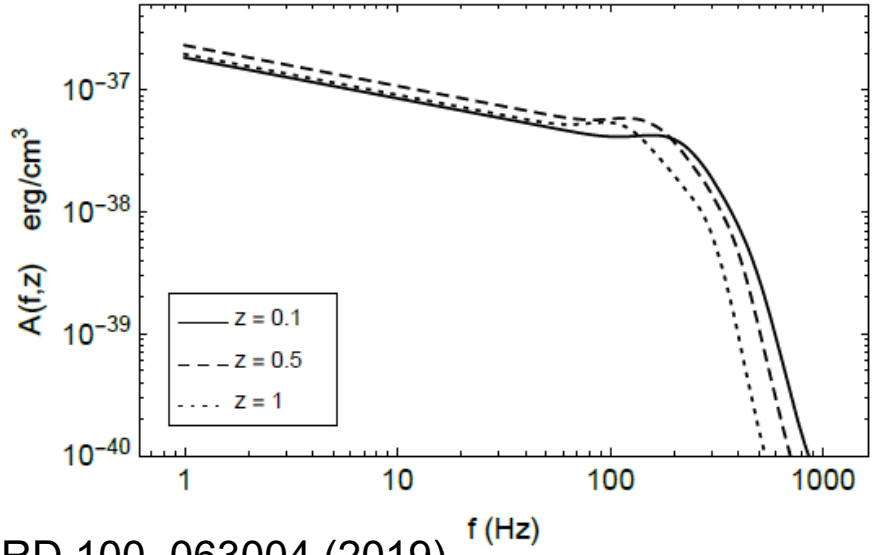

PRD 96, 103019 (2017); PRD 100, 063004 (2019).

Theoretical Modeling of Anisotropy: Compact Binaries

SGWB angular power spectrum

Cusin et al, Phys. Rev. Lett. 120, 231101 (2018)

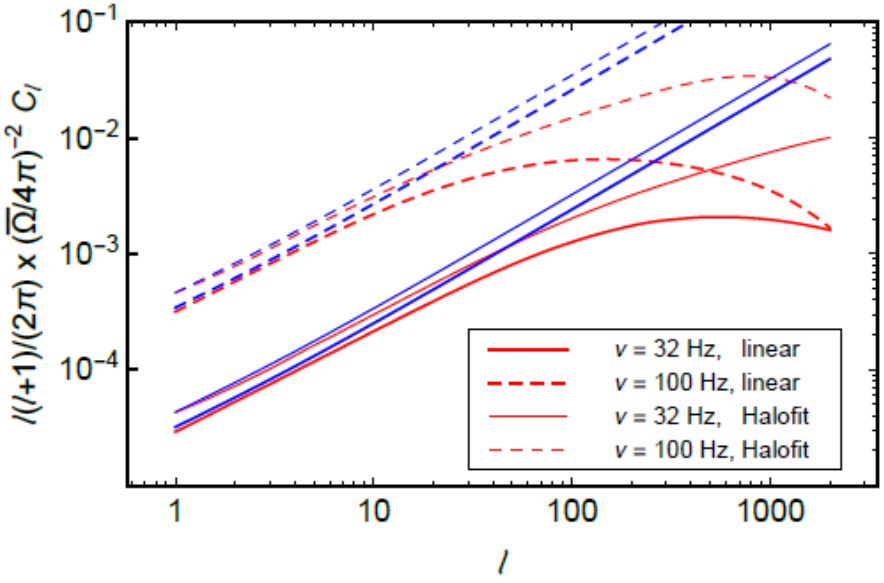

FIG. 2: Angular power spectrum of AGWB density fluctuation normalized to the monopole, for linear and non-linear (Halofit) spectra of density fluctuations. The straight blue lines are the associated large scale approximations (8).

SGWB-Galaxy Count angular power spectrum

G. Cusin et al., Phys. Rev. D 100, 063004 (2019).

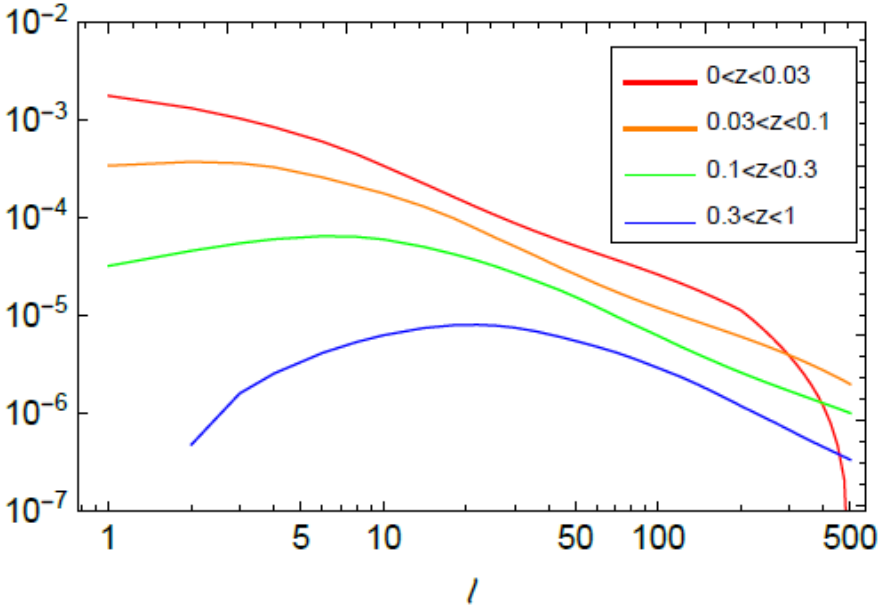

Cosmic Strings SGWB Anisotropy

- Topological defects generated during phase transitions in the early universe.
- Or, string theory strings.
- Cusps and kinks produce GWs.

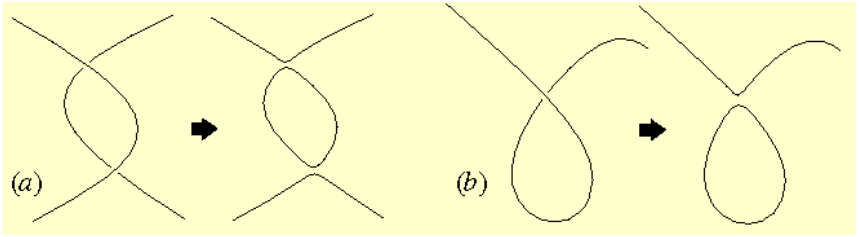

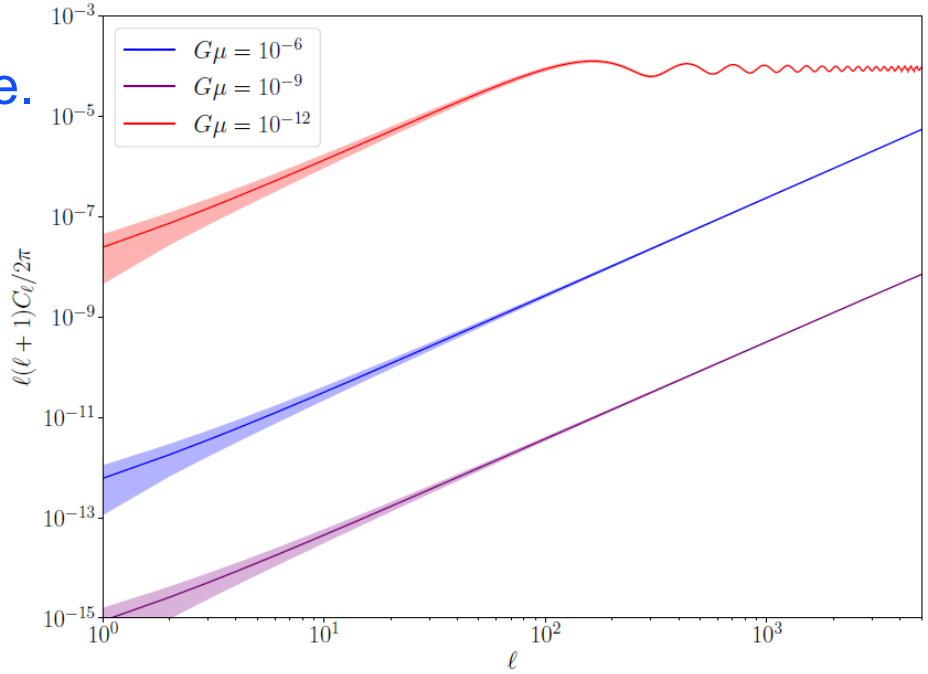

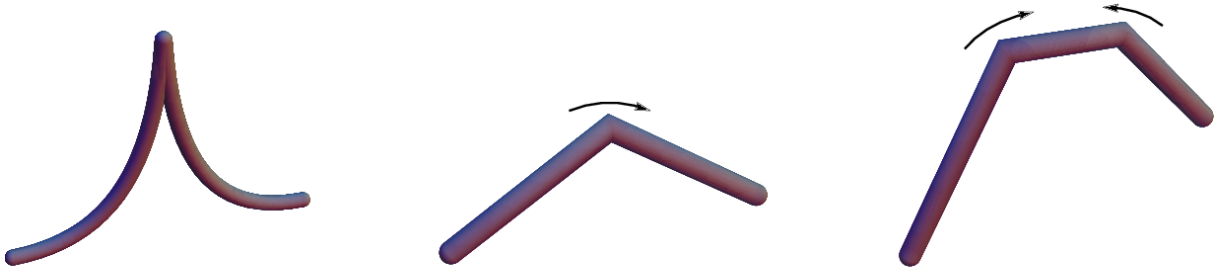

Cusp Kink Kink–Kink Collision

A.C. Jenkins and M. Sakellariadou, Phys. Rev. D 98, 063509 (2018)

GW-EM Correlations

O2 LIGO SGWB sky maps

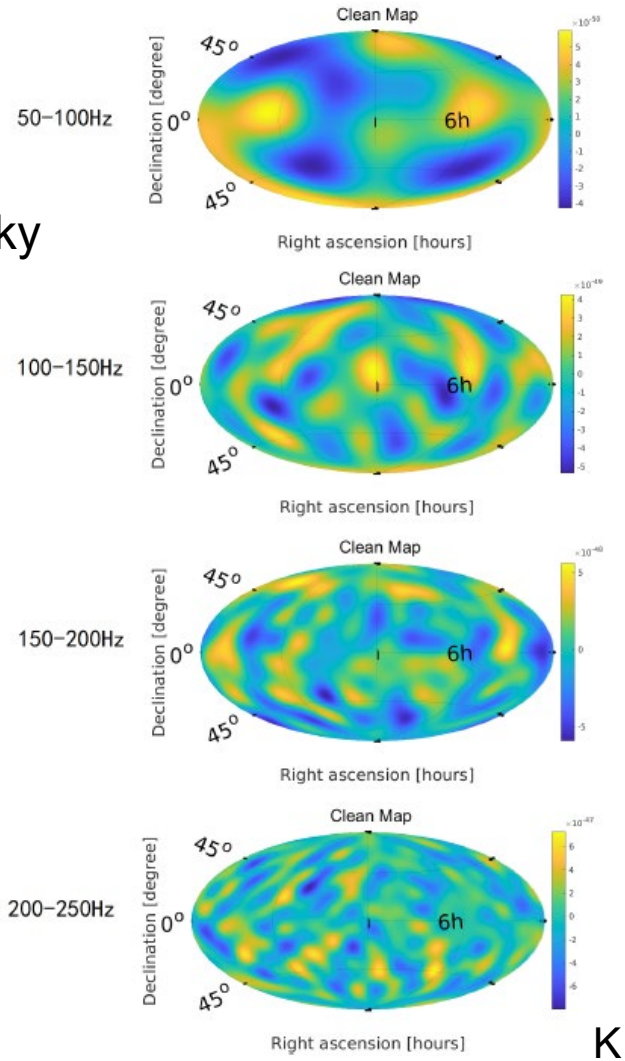

SDSS Galaxy Count Distribution

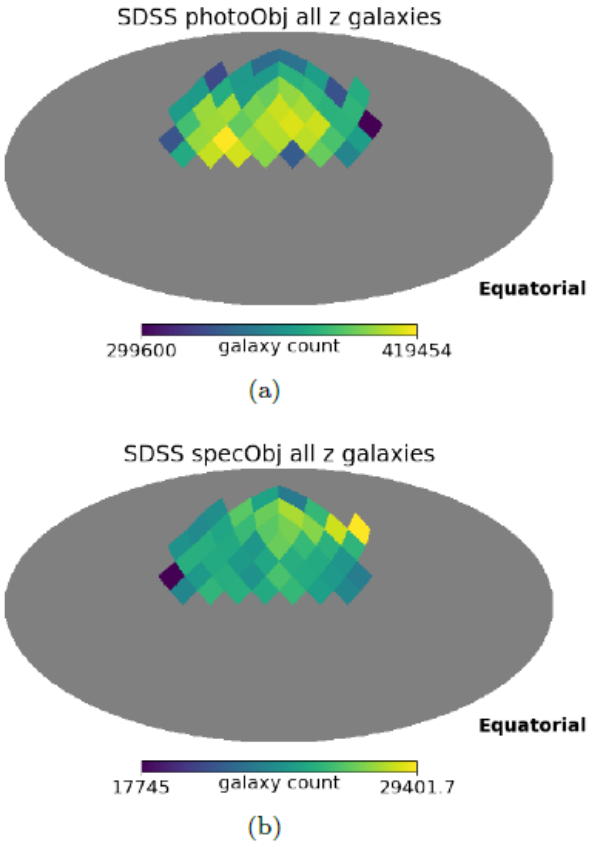

K.Z. Yang et al, MNRAS 500, 1666 (2021)

GW-EM Correlations

$$\Gamma = \frac{\langle \delta M_{\rm GW} \cdot \delta M_{\rm GC} \rangle^2}{\langle \delta M_{\rm GW}^2 \rangle \langle \delta M_{\rm GC}^2 \rangle}$$

p-values for observed Γ for different GW frequency bands and GC redshift bins

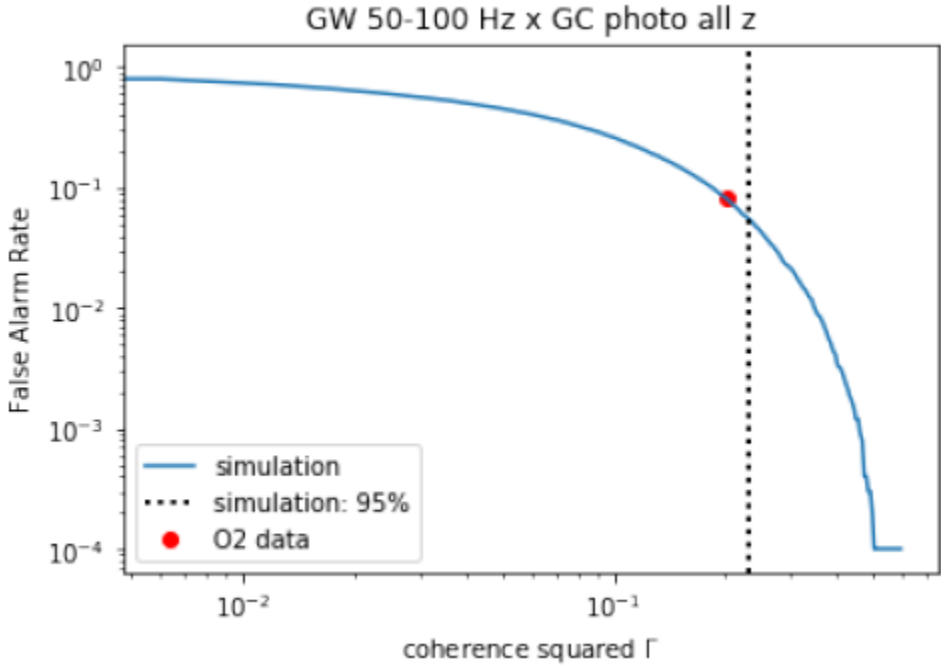

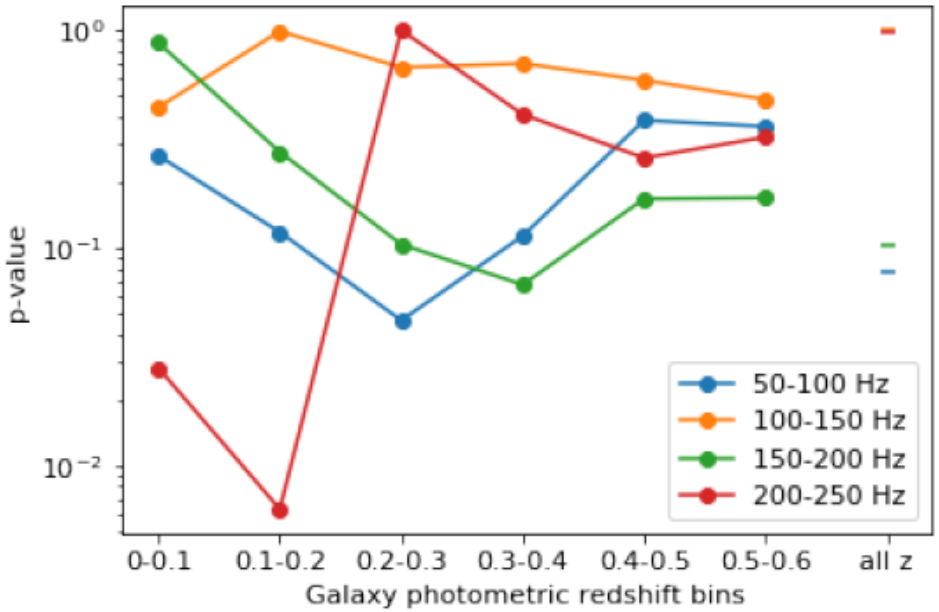

K.Z. Yang et al, MNRAS 500, 1666 (2021)

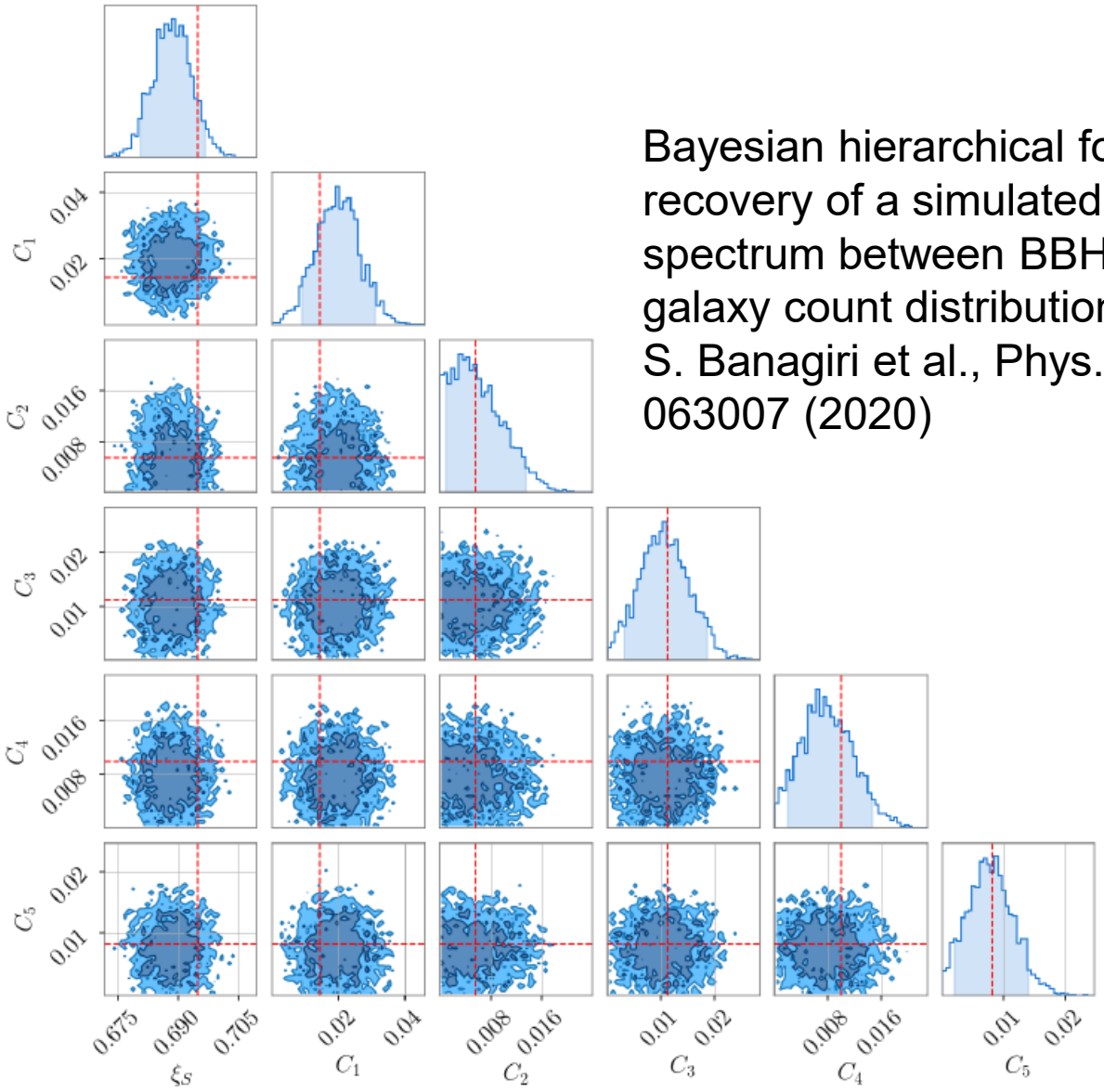

Bayesian hierarchical formalism allows for recovery of a simulated angular power spectrum between BBH population and the galaxy count distribution.
S. Banagiri et al., Phys. Rev. D 102, 063007 (2020)

FIG. 3. Plot showing the recovered $\{C_\ell\}$ as well as the duty cycle factor ξ_S using BBH-Galaxy two-point correlations with 2.2×10^4 data segments and $\ell_{max} = 5$. The monopole term is not an explicit parameter since it is normalized over and all other C_ℓ are normalized against it. We use uniform priors on both ξ_S and $\{C_\ell\}$; 0 to 1 on the former and 0 to 0.1 on the latter. The shaded regions in the 1-d posteriors correspond to symmetric 90% confidence intervals. The dashed red lines are the true values of the injected parameters with $\xi_S = 0.7$ which corresponds to 15.4×10^3 BBH signals and $(C_1, C_2, C_3, C_4, C_5) = (0.014, 0.006, 0.011, 0.01, 0.008)$.